UNIVERSITAT POLITÈCNICA DE VALÈNCIA

motores térmicos

TRABAJO DE FIN DE MÁSTER

ESTUDIO DE LA INYECCIÓN Y COMBUSTIÓN DIESEL MEDIANTE LA APLICACIÓN DE TÉCNICAS DE VISUALIZACIÓN Y MEDIDA

Realizado por: D. Carlos Micó Reche
Dirigido por: Prof. D. José Vicente Pastor Soriano

Valencia, 2 de julio de 2012

Máster Universitario en
Motores de Combustión Interna Alternativos

INSTITUTO UNIVERSITARIO DE INVESTIGACIÓN CMT-MOTORES TÉRMICOS

1. Introducción

En la actualidad, el empleo de técnicas de visualización y medida para el estudio de la combustión diesel está muy extendido. Esto ha sido posible, por un lado, gracias a la continua evolución del equipamiento y las herramientas disponibles, lo que ha incrementado el potencial de estas técnicas y ha permitido el estudio de fenómenos imposibles de analizar por otros medios. Por otro lado, gracias las ventajas que presentan, como resolución espacial y temporal o el destacable carácter no intrusivo de las mismas.

Existe una gran variedad de técnicas de visualización, basadas en diferentes aspectos físicos y químicos del propio combustible y de las reacciones que tienen lugar dentro de la cámara de combustión de un MCIA. Así, el grado de complejidad de éstas puede variar considerablemente, dependiendo tanto del montaje experimental que requiere como del fenómeno que se vaya a estudiar.

El interés actual de la investigación en los MEC reside principalmente en una búsqueda por reducir la formación de óxidos de nitrógeno (NOx) y partículas sólidas de hollín, de acuerdo con las directrices cada vez más estrictas de las diferentes normativas internacionales. Para ello se hace necesario incrementar el conocimiento en todos los fenómenos involucrados en el proceso de inyección y combustión del gasóleo. Esto involucra procesos muy distintos, desde la atomización, evaporación y mezcla del combustible con el aire hasta la aparición de las primeras reacciones o la formación de hollín dentro de la llama.

El correcto estudio de todos estos procesos hace necesaria una correcta selección de las técnicas de visualización y medida a emplear, basándose en la fenomenología físico-química de cada proceso. Es en este contexto en el que se engloba esta tesis fin de máster, en el cual se van a presentar diferentes estudios basados en la aplicación de variedad de técnicas de visualización y medida para el análisis de diferentes aspectos característicos del chorro gasóleo y su combustión.

2. Memoria

Los tres trabajos de investigación que se presentan en esta tesis han sido llevados a cabo durante el período de docencia del Máster en Motores de Combustión Interna Alternativos. Todos ellos se enmarcan en diferentes colaboraciones con empresas del sector de la automoción y quedan reflejados en una publicación enviada (JCR) y dos informes técnicos, que se adjuntan como anexos a este documento.

Como se ha visto en la introducción, la completa caracterización de la combustión gasóleo requiere del estudio de los diferentes fenómenos que tienen lugar durante el proceso de inyección y combustión en un MEC. El trabajo que se presenta a continuación comprende el análisis diferentes procesos o "etapas" involucrados, mediante la aplicación de las correspondientes técnicas de visualización y medida más adecuadas. Así, la estructura de la memoria es la siguiente:

2.1 Medida de velocidad y diámetro de gotas mediante Phase Doppler Particle Anemometry (PDPA).

2.2 Medida de magnitudes características de la llama gasóleo como temperatura, hollín o longitud Lift-Off, mediante aplicación de varias técnicas de forma simultánea.

2.3 Estudio del proceso de combustión mediante espectroscopia UV-Visible.

2.1 Medida de velocidad y diámetro de gotas mediante *Phase Doppler Particle Anemometry* (PDPA)

Este estudio forma parte de un proyecto cuya finalidad es la caracterización completa de un inyector prototipo, desde el punto de vista de su desempeño e influencia en el proceso de inyección y combustión gasóleo. La principal ventaja que ofrece este nuevo inyector es la posibilidad de actuar directamente sobre el levantamiento de la aguja. Es por esto que en este trabajo se analiza la influencia que diferentes levantamientos de aguja, para diferentes condiciones de operación, puede tener sobre el diámetro y la velocidad de las gotas del chorro gasóleo.

Para ello se ha hecho uso de la técnica conocida como Phase Doppler Particle Anemometry . Esta se basa en registrar la dispersión de dos haces láser por parte de las gotas de gasóleo, lo que permite obtener medidas de velocidad y diámetro de cada una de las gotas. El trabajo se ha realizado en una maqueta experimental, con atmósfera de gas hexafluoruro de azufre (SF6) a baja presión (6 bar) y temperatura ambiente. Esto permite alcanzar alta densidad, bajo condiciones no evaporativas y garantizando una atmósfera inerte.

La aplicación de PDPA para la medida de velocidad y diámetro de gotas de un chorro de gasóleo en condiciones no evaporativas es complicado, debido a la densidad de gotas que se dan en la zona de medida. Sin embargo, ha sido posible obtenider medidas de velocidad y diámetro de gotas en varias secciones del chorro a lo largo de su eje, para diferentes condiciones de levantamiento de aguja, presión de inyección o densidad de la atmósfera. Las conclusiones más relevantes que se pueden sacar son:

- Ha sido posible caracterizar mediante PDPA la distribución de velocidad y diámetro de gotas en un chorro de gasóleo.

- Mayores levantamientos de aguja implican mayor velocidad de gotas

- Los efectos de la presión de rail o la densidad ambiente sobre la velocidad de las gotas se ven afectados por la modificación del nivel de levantamiento de la aguja.

2.2 Medida de magnitudes características de la llama gasóleo como temperatura, hollín o longitud Lift-Off, mediante aplicación de varias técnicas de forma simultánea.

El objetivo del trabajo que se presenta en este anexo es la elaboración de una base de datos completa sobre distintos parámetros característicos del proceso de combustión para varios combustibles simples (decano, hexadecano y tres mezclas binarias de los primeros). Estos parámetros son el tiempo de retraso de autoencendido, la longitud Lift-Off, la formación de hollín y la temperatura de la llama.

Para ello se hace uso de una combinación de varias técnicas, lo que permite medir las magnitudes mencionadas de forma simultánea. El tiempo de retraso del autoencendido se mide gracias a un fotodiodo que registra la luz que se emite desde la cámara de combustión. La longitud de Lift-off se obtiene registrando la quimioluminiscencia del radical OH, mediante el uso de una cámara intensificada junto con un filtro que solo permite registrar la radiación característica de este radical (en el ultravioleta). Por otro lado, para la medida de hollín se emplean tres técnicas de forma simultánea, pudiendo así combinarlas y solventar los inconvenientes que presentan por separado. Estas son *Laser Induced Incandescence* (LII), *Light extinction measurement* (LEM) y *2-Color Pyrometry*. Esta última, además, permite la obtención de la temperatura de llama.

Este trabajo se ha llevado a cabo en un motor monocilíndrico experimental, que presenta una culata modificada con tres accesos ópticos que permiten visualizar directamente la cámara de combustión. En esta instalación el aire dentro del cilindro puede alcanzar temperaturas por encima de los 900K y presiones de hasta 75bar durante la inyección, permitiendo así realizar un amplio estudio paramétrico para los combustibles mencionados. Este comprende 3 presiones de inyección, 3 presiones en el cilindro en PMS y 2 temperaturas en cilindro en PMS, para cinco combustibles diferentes.

Las conclusiones más importantes que se pueden extraer del trabajo experimental realizado son las siguientes:

- Se han aplicado 5 técnicas diferentes de forma simultánea. Esto va a permitir combinar los resultados de forma directa, para realizar un análisis completo del proceso de combustión.

- La combinación de todas las técnicas junto con los puntos del estudio paramétrico, para los cinco combustibles, va a permitir elaborar una extensa base de datos. Esto se traduce en un total de 130 condiciones distintas de ensayo.

El anexo correspondiente que acompaña a este documento únicamente se presenta una descripción del trabajo experimental. Esto es debido a que se finalizó recientemente y los primeros resultados se están obteniendo actualmente.

2.3 Estudio del proceso de combustión mediante la aplicación de Espectroscopia UV-Visible

En este trabajo se presenta la espectroscopia UV-Visible como una técnica de visualización y medida con potencial para el estudio de nuevos modos de combustión. En los últimos años han aparecido nuevas estrategias basadas en promover la combustión en condiciones de baja temperatura y baja concentración de combustible. Estas ofrecen varias ventajas frente a la combustión gasóleo convencional pero también presentan inconvenientes. Es necesario, por tanto, profundizar en la fenomenología de las reacciones que tienen lugar para poder mejorar en la comprensión de las mismas.

Con este objetivo se ha empleado la espectroscopia UV-Visible para el estudio de un modo de combustión llamado *SACI* (Spark assisted compression ignition), el cual está siendo desarrollado por parte del instituto CMT – Motores Térmicos en colaboración con una importante multinacional del sector automovilístico. El trabajo se ha llevado a cabo en un motor Diesel monocilíndrico de cuatro tiempos, equipado con un pistón alargado que permite albergar un espejo y acceso óptico de zafiro en la base del pistón, de forma que es posible visualizar directamente dentro de la cámara de combustión. Gracias a esto es posible combinar el diagnóstico a través del análisis de la señal de presión dentro del cilindro, con la visualización directa de la combustión a alta velocidad y la información obtenida del análisis de la radiación natural de la reacción mediante espectroscopia UV-Visible. Con ello es posible elaborar una descripción detallada de la evolución espacial y temporal que sigue la combustión dentro del cilindro.

Las conclusiones más importantes que se ha podido extraer de este trabajo son las siguientes:

- La espectroscopía UV-Visible se ha mostrado como una herramienta con potencial para el estudio de nuevos modos de combustión. Las conclusiones gracias a esta información concuerdan con lo observado a través del análisis de la señal de presión y de la visualización directa de la combustión.

- Basándose en la evolución de especies químicas como los radicales OH y CH, se ha podido elaborar una descripción del proceso de combustión SACI.

- Se ha identificado como principal ventaja de esta técnica la resolución en longitudes de onda, pudiendo identificar diferentes especies químicas al mismo tiempo. Por otro lado, como desventaja principal es la dificultad que presenta para obtener resultados cuantitativos.

Estos resultados se van a publicar y han sido enviados a una revista indexada JCR **(Applied Energy)** con el título ***"A Spectroscopy Study of Gasoline Partially Premixed Compression Ignition Spark Assisted Combustion"***

3. Anexos

3.1 Informes

3.1.1 PDPA Measurements on the Continental Direct Acting (CDA) Injector

PDPA Measurements on the Continental Direct Acting (CDA) injector

Raúl Payri, Carlos Micó
CMT-Motores Térmicos. Universidad Politécnica de Valencia. Spain

ABSTRACT

Diesel droplet velocity and diameter values of the Continental Direct Acting injector are investigated in order to analyze the effect of the different needle lifting percentages on these two parameters under different test conditions. PDPA technique, assuming its uncertainty and limitations, was applied to obtain the velocity and diameter measurements at several spray axial and radial positions.

Injector charge (needle lift), injection pressure and ambient density were varied. The correlations between them and particle velocity and diameter produce experimental trends that have been analyzed.

The results show that higher needle lift percentages imply higher droplet velocities. Moreover, if the combination with other test variables is analyzed more conclusions are obtained, related with higher ambient density and rail pressure. Regarding droplet diameter, measurements are not clear in some cases and do not provide all the necessary information to draw some conclusions.

INTRODUCTION

Currently, one of the most important objectives for automotive research during the last decade is reducing engines fuel consumption and pollutants. Its importance has increased during last years due to the economical and environmental situation that this society is living nowadays.

In the quest of improving the diesel engine performance and efficiency it is obvious that a great effort should be concentrated on the injection process, which is the main responsible for achieving a good air and fuel mixture. Several studies are focused on the optimization of injection strategies that allow diesel engines to meet current and future emission regulations without affecting the engine performance [2, 7]. One strategy, in continuous development in recent years, consists in not only controlling the number of injection but also the "shape" of the injection event. One way to achieve this is by controlling directly the needle lift position using a piezoelectric stack. This allows the control of the flow behavior inside the nozzle during the injector event. To implement this type of injection control, precision injectors have been developed.

The aim of this task is to use an experimental technique to analyze the influence of a direct acting injector on the Diesel spray development. Measuring particle size and velocity in optically dense sprays, like the Diesel ones, is a very challenging task. The phase Doppler particle analyzer (PDPA) is technique based on Diesel droplets light refraction of laser light which allows obtaining velocity and diameter values of every single droplet measured.

PDPA measurements are performed obtaining droplet velocity and diameter values, at different positions inside a spray, for a new prototype injector (7-hole sac nozzle) with direct needle control. The spray has been analyzed at several injection pressures; ambient density and different max needle lift percentages.

The first part of this report presents information about PDPA fundaments, its theory and state of art founded at the literature. The next section contains information about the different aspects related with the experimental set up like the test rig, the PDPA system. The third part of this report is an explanation of the test plan. The fifth and sixth sections present velocity and diameter results and analysis. The last part of the document is dedicated to conclusions about the application of the technique and the results analysis.

STATE OF ART OF PDPA TECHNIQUE AND CONCLUSIONS FROM LITERATURE REVIEW

Given the generally accepted difficulty of the PDPA application for Diesel jets, in the following paragraphs there will be presented a review of other researchers' work where this technique was used to characterize Diesel sprays.

The high density of the Diesel spray is a physical limitation for the PDPA technique that can only be overcome if the measurement volume is small enough to allow for the multiple droplet presence inside of it to be avoided. There are however other system parameters that also have to be chosen properly in order to eliminate noise and erroneous measurements. It can be noticed in the literature that the

authors are generally choosing to make the measurements and obtain their conclusions in areas of the spray where the droplet density is lower.

Hung et al [1] made measurements with a 240 μm orifice nozzle with two injection pressures: 21 MPa and 105 MPa. It was observed that at 10 mm and 20 mm from the orifice measurements on-axis with the high injection pressure were impossible. Furthermore, the experiment was performed at ambient density, which allows for what could be considered a spray dilated spatially especially in the penetration direction, by comparison to how the it develops in the 10 to 20 times higher densities encountered in the combustion chamber [2].

Arrègle et al [3] chose experimental conditions closer to reality, with injection pressures from 30 to 110 MPa, and ambient densities from 10 to 30 kg/m3. They only used the PDPA to measure the SMD. This, although not stated clearly, indicates that they found rather difficult and unreliable the velocity measurements in the quasi-stationary part of the spray, and thus based the SMD data on the first droplets reaching the probe volume, measured before the injector opened completely and the spray became too dense. The spray front and its tail are easier to measure and might present valid diameter measurements but the velocity data is obviously much lower than in the main part.

Levy et al [4] performed SMD measurements at a relatively short distance from the orifice, 10 to 30 mm, but with a low injection pressure of 20 MPa and evaporative conditions with an atmosphere density of 9 kg/m3 and high temperature of 500ºC. There can also be found data about the system settings, revealing that the probe volume waist was 50μm, one of the lowest values encountered throughout the literature.

Koo and Martin [5], use a beam waist of 200 μm and slit of 50 μm that due to the optics has an actual size of 103.1 μm. They employ a low injection pressure between 15 and 25 MPa, explaining how they were able to measure as close as 10 mm to the orifice. However, it is not stated if the measurement points were on or off the axis. There is no data given about the ambient density but it must have been very low given the fact they measured velocities of 125 m/s very far from the orifice, at 120 mm.

Coghe and Cossali [6] performed a complex study with ambient densities between 0.95 and 18 kg/m3 and temperatures between 20º and 100ºC. The injection pressure was 70 MPa and the measurement points were located far from the orifice, at 52, 57 and 62 mm. The study was aimed at observing the SMD in evaporative conditions.

Araneo and Tropea [7] are the authors of an extensive work over the PDA system optimization for measurements in a Diesel spray. They used a measurement volume of 77 μm waist diameter, and a slit opening of 165 μm that due to the 30º scattering angle was projected at 330 μm on the probe volume. The measurement sections were located at 5, 50 and 100 mm from the injector in normal atmospheric conditions, which, according to the authors, due to the spray re-scaling, correspond to distances ten times smaller for a spray injected in 20kg/m3 ambient density. At 5 mm from the orifice the measurements were impossible on-axis. There was investigated the influence of various system parameters like the laser power, the signal-to-noise ratio, the photomultipliers voltage and the applied threshold. The scattering angle was chosen at 30º because it allows for higher scattering intensity, but it requires for a well known and stable refraction coefficient, conditions met in a non-evaporating diesel jet. However the 70º setting could also be chosen because it has the advantage of reducing the system sensibility to refraction index. Generally angles between 30º and 75º insure the dominance of the first order refraction.

Strakey et al [8] performed a study on rocket jets that also holds promise for the characterisation of Diesel sprays. The step forward is taken by employing a measurement volume slightly smaller than the average measured particle. There are many droplets that don't pass through the probe volume centre and reflect the beams instead of refracting them and thus have to be eliminated from diameter statistics, but this decrease in validation rate is more that counterbalanced by the increase owed to the avoidance of multiple droplet presence in the probe volume. The authors show that the erroneous diameter measurements can be almost completely eliminated by employing the intensity validation criterion. This insures that there is always agreement between the scattering intensity and the particle size, i.e. small particles with strong signals and big ones with weak signals are eliminated. The technique was tested and proved in a mono-disperse spray, and then applied to a rocket jet. The probe volume waist was 64 μm and the average diameter observed was around 80μm. For similar application to Diesel sprays the waist diameter should be reduced to approximately 20 μm.

Various authors explored the possibility of explaining the droplets size as a result of the established equilibrium between the aerodynamic friction forces and the superficial tension ones. According to this, the faster a droplet is travelling the smaller it should be, but as it was found in [7], [1] and [9] there is no correlation between velocity and size, and furthermore, the droplets corresponding to modern injection systems have much lower diameters than the equilibrium limit would suggest.

One of the conclusions upon which there seems to be general agreement is the one that the average diameter and the SMD increase with the distance to the orifice, in non-evaporative conditions, like for example in [10], [7] and [11]. As Smallwood and Gülder [12] observe in their review over the current Diesel spray structure knowledge, there seems to be now general agreement over the fact that the direct injection spray is fully atomized as it exits the nozzle or very near to it. It is thus concluded that droplet size redistribution downstream of the nozzle is mainly due to coalescence, and that although aerodynamic secondary break-up may occur it is far less important than previously thought.

There is also agreement over a set of intuitive dependencies, like the one of the SMD decreasing for higher injection pressures and for smaller orifice diameters. In [13] and [14] there is also noted that a sharp-edged orifice inlet produces lower SMD than a rounded inlet one. From [7], [15] and [5] it can also be drawn the conclusion that droplets diameter is higher on average at the spray centre.

Bachalo [16] provides a valuable insight to the application of PDPA to dense sprays. One of the critical aspects discussed is the droplet sphericity, which can lead to both underestimation and overestimation of the diameter, depending on the droplet's orientation. According to him, droplets of 100 μm or more are susceptible to deformation while in the case of smaller ones, typical for the actual Diesel spray, the surface tension is strong enough to maintain the sphericity. They also made the interesting point that if droplets oscillate randomly, the average size measured will be very close to the real one.

Velocity results are presented in a significantly lower number of papers, especially in those that performed the experiments in atmospheric conditions. Results in these conditions are spread in a 100 to 200 m/s range ([17], [7], [1] and [5]) for different combinations of injection pressures and penetration distances. The interesting point is that the validity of the results is never questioned; at best a system check is performed in a continuous flow of known velocity, which can indeed reveal if the measurements are correct but cannot simulate the difficult conditions of high droplet density encountered in a Diesel spray. Furthermore, the inherent system limitations, that surely all authors encountered, are not stated clearly and have not been properly analyzed so far.

WORKING PRINCIPLE OF PDPA SYSTEM

The core of the hardware part of the PDPA technique is represented by a laser system that emits one beam which is split into two or more components of equal intensity (Figure 1).

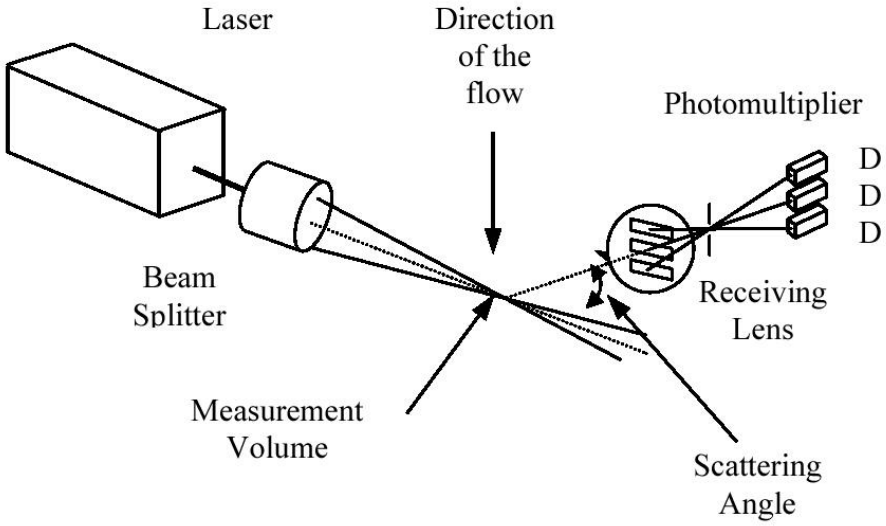

Figure 1. Scheme of a PDPA arrangement

A lens is then used to focus and intersect the beams at the point where measurements will be made. This point is called the measuring-, probe-, or control-volume. Interference of the light beams, which occurs due to a phase difference between the light waves, creates in the measurement volume a set of equally spaced fringes represented by alternative bright and dark bands (Figure 2).

Velocity and size measurements are made when a particle crosses these fringes. When a particle traverses the control volume, the amount of light received fluctuate with the fringes and so does the one scattered into the surrounding directions. This is then collected by another lens and focused on a photo-detector which converts the fluctuations of light intensity into a voltage signal. The frequency of this fluctuation is proportional to the velocity of the particle. This frequency is known as the Doppler Shift frequency given by:

$$f_d = \frac{2 \cdot v \cdot \sin\left(\frac{\gamma}{2}\right)}{\lambda} \qquad (1)$$

Where v is the velocity component of the particle normal to the fringes, γ is the crossing angle between the two beams and λ is the wavelength of the laser light.

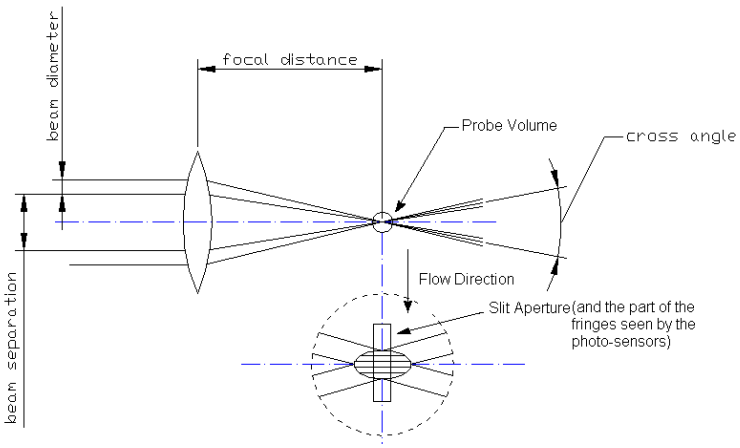

Figure 2. Main optical parameters in a PDPA system

The electronic signal given out by the photo-detector contains periods of silence randomly interrupted by bursts of signal (Figure 3). The overall shape of the burst is a consequence of the fact that the energy is normally-distributed along the laser beam diameter which produces the measurement volume, and as such they are stronger at their centre than at their edges.

As the particle passes through the edge of the measurement volume, where the fringes are weakly illuminated, the signal fluctuations are weak. As the particle passes through the measurement volume centre the signal fluctuations become larger and then decay again.

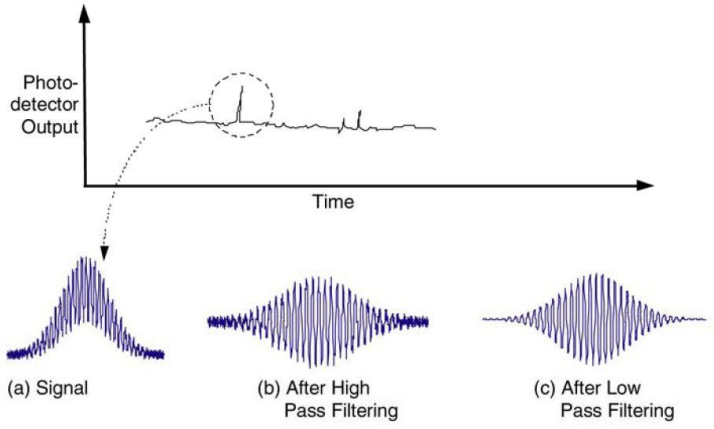

Figure 3. PDPA signal processing

The fluctuations are not centered about zero because light intensity cannot be negative. As a consequence the signal can be split into two parts: a low frequency part called the “pedestal” and a high frequency part that actually contains the Doppler signal. There are also higher frequencies that represent noise and have to be removed by a low-pass filter.

The Doppler frequency fd can be determined by measuring the period of the Doppler signal. If the laser wavelength and the angle of intersection of the two beams are known, the droplet velocity can then be calculated according to equation 1.

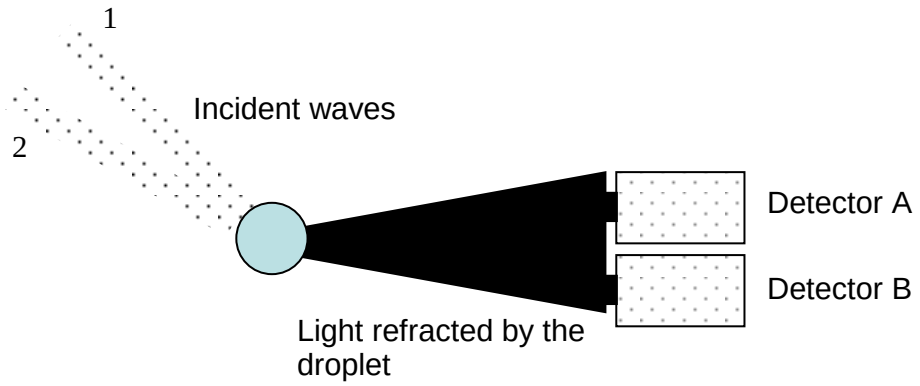

Figure 4. Diameter measurement in a PDPA system

Bachalo and Houser [18] showed that if two photo-detectors collecting light simultaneously are employed, the Doppler burst signal produced by each detector will be the same but with a phase shift between them. The phase difference $\Delta\varphi$ occurs due to the difference in the optical path that has to be taken inside the droplet by the incident waves 1 and 2 to reach each of the detectors A and B (Figure 4). The signals arriving at the detectors A and B have the same frequency but different phase:

$$I_A \approx E_{SC}^2 \cdot \left[1+\cos\left(2\pi \cdot f_d \cdot t - \frac{\psi_{1A}-\psi_{2A}}{2}\right)\right] \quad (2)$$

$$I_B \approx E_{SC}^2 \cdot \left[1+\cos\left(2\pi \cdot f_d \cdot t - \frac{\psi_{1B}-\psi_{2B}}{2}\right)\right] \quad (3)$$

$$\Delta\varphi = \frac{1}{2}\left(\psi_{1B}+\psi_{2A}-\psi_{2B}-\psi_{1A}\right) \quad (4)$$

For a given optical configuration, the phase shift is directly related to the particle size by a linear calibration curve. The slope of the linear response curve is dependent on the optical parameters, which consist of the laser wavelength, the collection angle, the laser beam intersection angle and the refractive index of the particle. In some cases, a phase shift greater than 360° could occur and the calibration curve is no longer valid. A third detector is used to recognize and remove such uncertainties. The third detector can also be used to eliminate sizing errors due to non-spherical particles or noise.

EXPERIMENTAL SET UP

INJECTION SYSTEM

A standard Common-Rail system is used for the experimental work. It is composed by a high pressure pump and a conventional Common-Rail with a pressure regulator, which allows working with a range of injection pressure up to 2000 bar (keeping it almost constant). The prototype injector used in the present study uses a piezoelectric actuator directly coupled to the nozzle needle, which allows a direct control of the needle position. The needle lift is proportional to the charge applied to the piezo stack. The characteristics of the nozzle are shown in Table 1. In addition, the injection system is directly controlled by the ECU.

Nozzle seat type	microsac
Conicity factor, K	1.5
Number of spray holes	7
Outside hole diameter, D0 (µm)	152
Discharge coefficient	0.81

Tabla 1. Nozzle characteristics

Accordingly with results presented during flow behavior characterization of CAD injector at CMT, only the hole number 2 is chosen for PDPA measurements. Considering the relative momentum coefficient calculated for the 7 holes, at different test conditions, this hole is the one which shows a similar behavior along the whole rail pressure range.

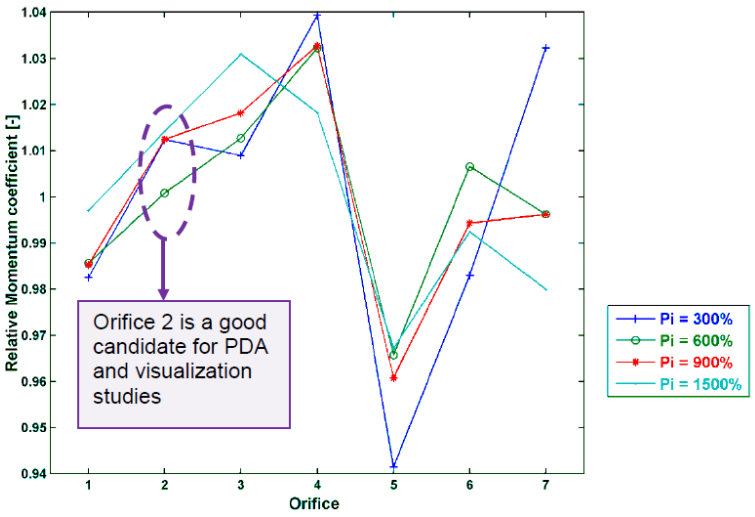

Figure 5. Relative momentum coefficient for 35% charge.

The direct study on the diesel spray in its usual environment, i.e. the engine, is more complicated due to the fact that optical access is restricted physically and that the eventual windows are easily dirtied when running the engine. One of the compromise solutions is to reproduce completely or partially the engine environment in a purpose-built test rig which can have larger dimensions and proper optical access. The present work will concentrate on spray studies realized in cold test rigs that are run at ambient temperature but have inside a pressurized gas. A brief description of this test rig is included below.

SF_6 INJECTION TEST RIG

The experiments have been performed in a pressurized test rig that offers better optical access than a normal engine but can still reproduce totally or partially the ambient conditions from the combustion chamber at the moment of injection. In the present case it was decided to reproduce only the density and not the temperature because this would have implied higher potential exposure to hazards.

The test rig is filled with a dense gas, sulphur hexa-fluoride (SF6), which is inert and thus combustion is surely avoided. Due to its high molecular mass it can reach the density values that normally occur in a Diesel engine at the moment of injection at much lower than for other inert gases like Nitrogen. It is generally accepted that the behavior of the spray only depends on the density of the ambient, not on its pressure, meaning that the experiments performed in such a test rig are representative of the real behavior of a Diesel spray [20].

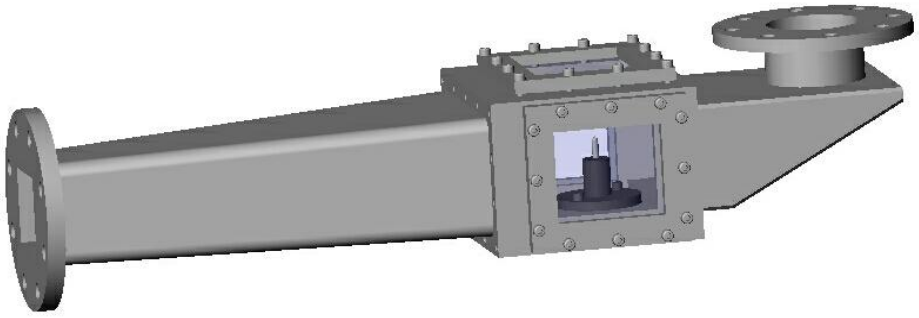

Figure 6. The test rig's section

The temperature inside the rig is constant, fixed at 25 ºC. The rig is of the closed-loop type, which means the gas is continuously circulated, passing through filters that remove the injected fuel and then through the roots compressor that sends it back to the actual testing section. The flow velocity next to the injector is lower than 3 m/s, so that it shouldn't affect the diesel spray, while also avoiding window fouling. The testing section of the rig is shown in Figure 6, where the three Plexiglas windows can be seen ensuring the optical access.

In order to study the spray evolution, only one jet from the injector nozzle needs to be allowed to develop freely, since the other ones are irrelevant and even inconvenient for the purpose of the study. In fact, the rig is difficult to operate with a multi-orifice injector, since the additional sprays cause the contamination of the windows, as they are generally directed towards them. Consequently, a special cap needs to be employed to collect all but the studied spray. Figure 7 shows and scheme of the device used for isolating the test spray. It can be observed that the rest of the sprays hit the cap avoiding also window fouling of the SF6 test rig.

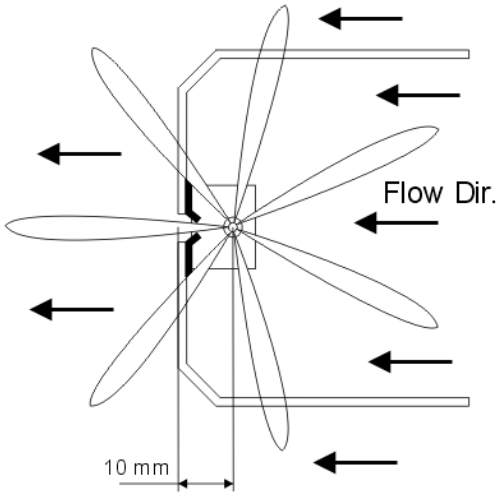

Figure 7. Scheme of the upper view of the spray isolation cap

A Roots compressor is used to provide a maximum flow rate of 5000 l/min, with an increase of about 0.05 MPa in the vessel pressure. Two filters collect the fuel injected in order to keep the gas stream clean; the first one is of the cyclonic type, and the second is one of higher efficiency, retaining the smaller droplets.

PDPA SYSTEM

The PDPA system configuration used for this task was obtained from the work presented by Soare at [19]. The author presents an optimization procedure which gives, as a result, an optimum configuration for PDPA technique applied to a Diesel spray with the equipment that CMT has. A description of the whole system and its configuration is presented below.

The laser source is a continuous 4 W "Ar+" laser, INNOVA 70c, produced by Coherent Inc. It is set to emit green light with 514 nm wave length. The laser beam emitted goes into an optical system composed by the Bragg cell and mirrors that direct the resulting beams upwards into the optic fibers. The Bragg cell operates at a frequency of 40 MHz, which induces the corresponding phase difference between the two beams. This causes the fringe pattern to move, preferably in the opposite direction of the measured flow. This has two positive consequences. The first is that a stationary droplet will be detected as it will produce a 40 MHz signal due to the fringe movement. The second is that it allows distinguishing between droplets that move in opposite directions, since the ones moving against the fringe pattern (and in the preferential direction of the flow) will produce a Doppler frequency higher that 40MHz and the others a frequency between 0 and 40 MHz.

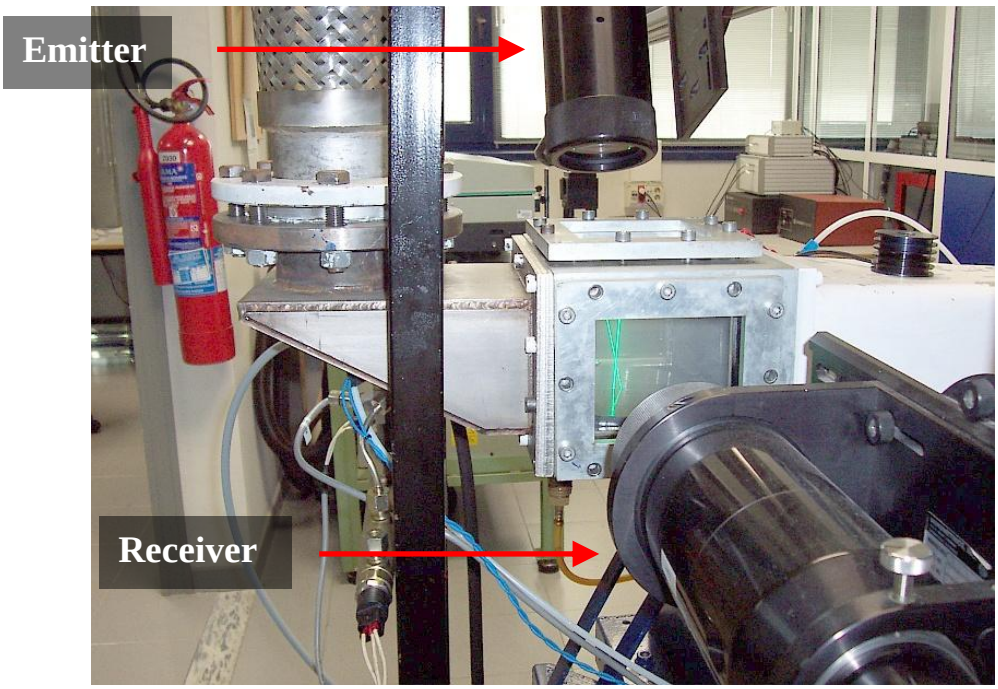

Figure 8. System optics position relative to the test rig

The optical components, i.e. the beam splitter, the emitter and the receiver, are built by Aerometrics. The main optical parameters are as follows:

- *Beam separation before beam expander: 40mm.*
- *Beam diameter before beam expander: 1.4mm.*
- *Beam expander ratio: 1.44.*
- *Emitters front lens' focal length: 200mm.*
- *Probe volume waist: 65μm. Fringe spacing: 1.805μm.*
- *Receiver front lens' focal length: 300mm.*
- *Receiver back lens' focal length: 250mm.*
- *Receiver lenses' effective diameter: 70mm.*
- *Slit aperture: 25μm.*

It should be specified here that due to the ratio between the receiver lenses' focal distances, the actual slit aperture focused on the probe volume is 30μm.

The signal processor is the key element of the system because it has the task of interpreting the analogue signals representing the droplets passing through the probe volume. These signals are arriving at a very high rate, especially in the case of a Diesel spray, are very short, have different

frequencies and are often overlapping one another. The main characteristics of the FSA 4000 processor, manufactured by TSI Inc., are:

- *Maximum measurable frequency: 175MHz (corresponding to 243.66m/s with current optical set-up).*
- *Minimum measurable frequency: 300Hz (corresponding to -72.19m/s with current optical set-up).*
- *Minimum transit time: 50ns (this imposes an upper velocity limit of 1300m/s)*
- *Maximum sampling rate: 800MHz.*

The system requires calibration for the diameter measurement, in order to make sure the considered phase difference between signals coming from the three detectors is only due to the presence of a particle and not to the various delays occurred in the processing chain. For this it employs a calibration diode that generates a signal with similar frequency and intensity to the average ones expected during a real measurement. Since it is the same signal arriving at exactly the same time to the three photomultipliers, the systematic phase differences are revealed and then included as correction factors in the diameter calculation.

The light signal originated from the droplet-scattered light is brought via optic fibers to the photomultipliers where it is transformed into an electric signal. Here there is also applied a high-pass filter that removes the pedestal (Figure 3). The user can chose between two high-pass filters: 5MHz and 20MHz.

The pedestal-removed signal's frequency is then decreased by a quantity between 0 and 40MHz that is also chosen by the user. This is called downmixing. It consists on multiplying or "mixing" the input signal with the downmix frequency selected in the software. The resulting signal then has two frequency components: the sum and the difference of the input and the mix frequencies. As it is suggested by Soare at [19], is recommended to set the downmixing freq. at 0. This ensures that data is discarded because in a Diesel spray normally a big range of velocities are present.

The user can chose from twenty bandpass filters to remove noise. The resulting filtered signal can be observed by connecting an oscilloscope to a BNC connector on the front panel of the processor case. There are combinations of flow speed, filter choice and downmix frequencies where the "difference" component is eliminated and the "sum" kept, making it appear as the correct one. This leads to measuring velocities that are much higher than the real ones.

After going through the bandpass filters, the signal splits into two: one goes to the burst detector and the other to the burst sampler. The burst detector's task is to flag the beginning and end of a possible Doppler burst signal from the continuous background noise. The burst detector discriminates between the Doppler signal and the background noise by continually monitoring the signal-to-noise ratio (SNR) of the incoming signal and detecting when the signal exceeds the value set in the software. The detector performs this task by first digitizing the signal and then performing a real time Discrete Fourier Transform (DFT) and a comparison with a set of look-up tables (LUT). When a signal exceeds the preset SNR level, a burst gate is started and a timer in the burst detector measures the duration of the signal. At the end of it, the burst gate is stopped and the measured duration is used to determine the centre of the burst.

The burst detector relies also on an amplitude-based threshold for selecting only the larger amplitude signals with good SNR. The burst detector's control logic combines all these inputs to determine when to turn on and off the burst gate. This burst gate output is a rectangular signal that is also available from a BNC connector on the front panel. The FSA stores the current value of the time stamp counter and the current value of any external input data requested at the end of the burst gate. Later, this data is paired up with the other data processed from that burst. The burst detector also keeps track of how long the burst gate was on, and this becomes the transit time or gate time data for each burst. This burst gate identifies the best region of the burst from which to collect samples. The optimum sampling rate combines with the output of the burst gate to collect the best samples to send to the burst processing section.

The burst processing is done by four digital signal processing (DSP) chips for each channel, so all the burst processing is performed in the FSA signal processor. The computer is only used to run the control software and display the data, and thus the performances required from it are minimal. Burst processing consists of determining the frequency of a signal and measuring the phase difference between channels 1A, 1B and 1C. The digit used in this nomenclature represents the velocity component and the letters stand for the three detectors used for the diameter measurement. Burst processing also involves determining if the burst is valid or not, based on the SNR level selected in the software. Only burst data passing this validation step is sent to the computer.

The displayed hardware data rate indicates the number of valid bursts per second. Hence, not every burst that creates a gate is accounted for by the data rate. The displayed burst efficiency is the ratio of valid bursts to burst gates. It is a good indicator of how noisy the signal is, or how good the selected settings are. Once a signal is processed, it is sent to the computer with its frequency, time stamp, transit time, channel number, phase AB (phase difference between signals A and B), phase AC, and intensity. In addition, it is also able to include any external input data, like crankshaft angle, temperature, pressure, etc.

Summarizing, the parameters that affect the way data is recorded, and thus cannot be changed after the experiment is finished are: the high-pass filter that acts on the signal generated by the photomultipliers to remove the pedestal, the bandpass filter, the downmix frequency, the burst threshold, the SNR and, obviously, the PMT voltage. According to values suggested by Soare at [19] for a Diesel spray measurement, the values selected for the results presented at this report are:

Laser Power	850 mW
PMT voltage	550 V
Frequency band filter	40-120 Mhz (0 - 144 m/s)
Bragg Cell frequency	40 Mhz
Downmix frequency	0 Mhz
Burst Threshold	200 mV
SNR	"Very Low"

Table 2. PDPA system software parameter

AXIS LOCATION

A big difference between working with a single hole or a multiple hole injector is that the first one can be installed in a position that the spray axis is aligned with the movement axis of the coordinate bench were PDPA optics are installed. This fact makes necessary to locate the spray in order to obtain a matrix of the different test positions but referred to the coordinate bench axis.

The procedure is based on several scans, made at sections at different distances from the nozzle. At each one, droplet velocity is measured all along it obtaining a mesh of velocity values. Having a good spatial resolution is very important to ensure that the point of the spray axis is registered. In this case, an interval of 0.25 mm was used. Figure 9 and Figure 10 show the result from scans at 20 mm and 50 mm from axis.

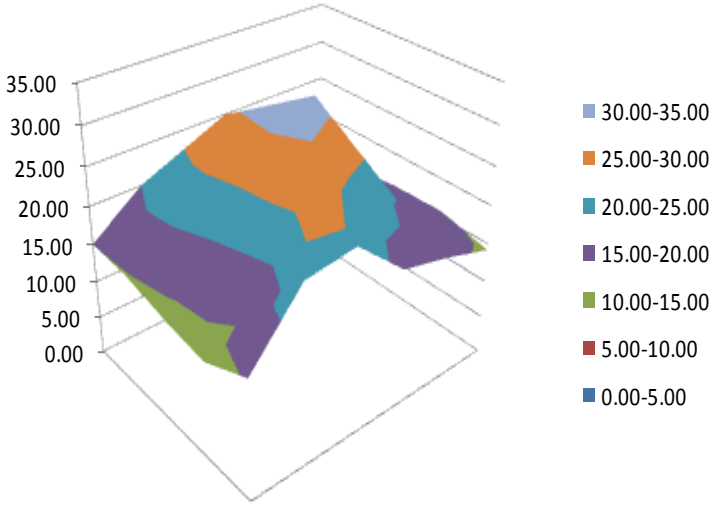

Figure 9. Velocity map generated from a scan at 20 mm from the nozzle.

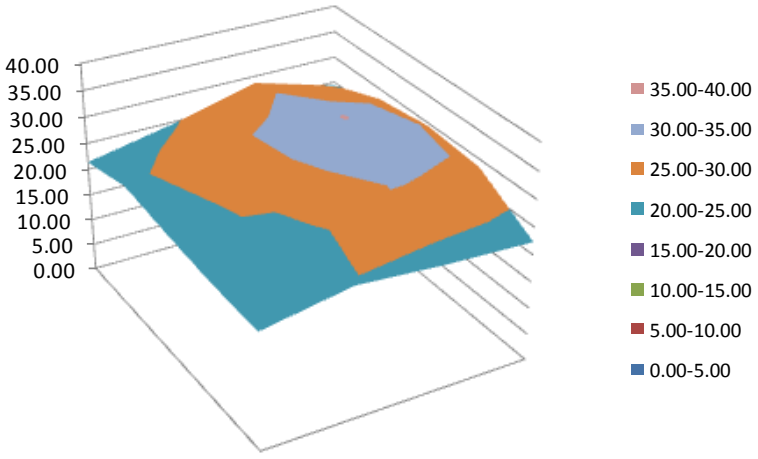

Figure 10. Velocity map generated from a scan at 50 mm from the nozzle

The criteria followed to consider a point of a section as the one which belongs to the spray axis is related to the velocity value measured. The position where the highest velocity is measured is considered as part from the spray axis. Once that two or more points are found, the equation for the spray axis can be obtained and thus the equations for the sections of interest.

Knowing the axis equation, it is possible to calculate the spray included angle and its complementary. If the injector is positioned perpendicular to what is considered as horizontal plane, it is only necessary to calculate the angle between the studied spray and this plane. As a result, 11.68º was obtained. The injector geometrical specifications establish that this angle should be 12º. Both values are very similar which means that the axis defined by the technique described above is reasonable.

PDPA TEST PLAN

For the analysis of injector charge influence on the droplet behavior test conditions were chosen from the test plan presented Mass flow rate and Momentum Flux test plan. Two rail pressures and two ambient densities are tested in order to obtain information about the charge effects at different test conditions. The test condition matrix is presented in the next table.

Nº Injections	Shape	Rail pressure	ET	SF6 Pressure	C_Cur_Cha_Man		Total points
					10 Hz	0.3 Hz	
[-]	[-]	[bar]	[µs]	[bar]	[%]	[%]	[-]
Single	Square	600	3200	3.25	22.5	23.79	1
Single	Square	600	3200	3.25	25.0	26.00	1
Single	Square	600	3200	3.25	30.0	30.90	1
Single	Square	1500	3200	3.25	25.0	26.00	1
Single	Square	1500	3200	3.25	27.5	27.69	1
Single	Square	1500	3200	3.25	30.0	30.75	1
Single	Square	1500	3200	6.25	25.0	26.00	1
Single	Square	1500	3200	6.25	27.5	27.69	1
Single	Square	1500	3200	6.25	30.0	30.75	1
TOTAL	9						

Table 3. Test conditions

The ambient density is established by the SF6 pressure inside the test rig, necessary for obtaining the desired values: 3.25 bar corresponds to 20 kg/m3 and 6.25 to 40 kg/m3. The rail pressure varies from 600 bar to 1500 bar to represent low and high injection pressures conditions. But for high density only the second value is tested because it was considered that under this ambient conditions, 600 bar would imply really low droplet velocities.

An injection frequency of 10 Hz is too high for working on the SF6 test rig. The atmosphere inside it is renewed thanks to a root compressor and two fuel filters, but the speed of the gas has to be low enough to avoid any influence on the injection process. That is the reason why tests were made at 0.3 Hz so charge values were changed in order to obtain the same injection behavior (at least the same Mass flow rate).

The energizing time is set to 3200 µs to maintain the stabilized stage of the spray the enough time to make PDPA measurements. A single square pulse is established to simplify the problem because the aim of this task is to study the central stabilized part of the spray.

For characterizing the whole spray, different points along the axis and on it section were chosen. Over the axis, measurements were taken at 30, 40, 50 and 60 mm from nozzle. For more than 60 mm droplet velocity would be to low due to the ambient density so measurements there are not useful. For distances smaller than 30 mm, the high speed of droplets and the amount of them present many problems for PDPA technique (in non evaporative conditions) so it would be very difficult to measure in that region of the spray. Moreover, due to the fact that the probe volume is generated by two laser

beams crossing themselves at the same point, it exists the possibility that for positions near de spray isolator device, one of the beams could be interfered by it.

Three points at a section of the spray were tested, at 40 and 50 mm from the nozzle. The distance chosen between them and the axis was 1 mm, which will allow obtaining a good spatial resolution. In the next figure, an scheme of all the test positions is shown. It can be seen also that the off-axis points were measured in the same side of the spray. This configuration was chosen considering that both emitted and scattered light have to cross the less possible amount of droplets for avoiding signal noise at the photomultiplier.

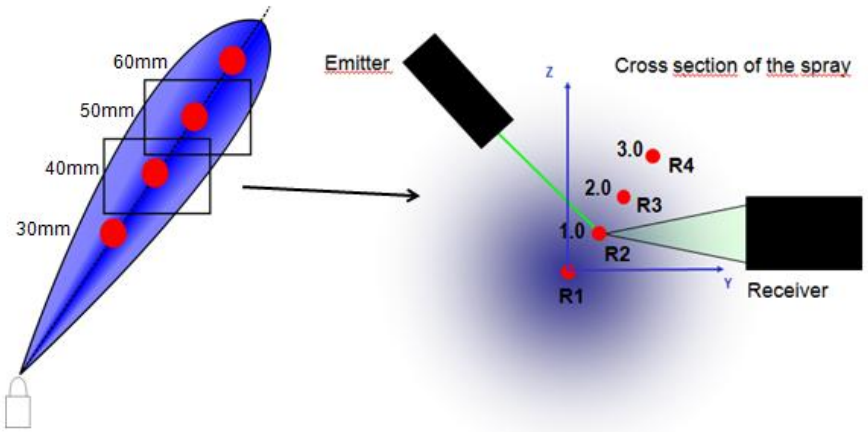

Figure 11. Scheme of the test positions selected

DATA ADQUISITION

The length of every test can be defined by total time or by maximum number of droplets found. For Diesel spray, due to the fact that is very difficult to measure a big amount of droplets, usually the first condition is defined for establish the duration. As it is exposed at [19], 5 minutes per test are enough for measurements.

Each PDPA test is composed by more than one injection. With the configuration chosen for this task, each test contains data from 100 different injections (0.3 Hz during 300 seconds). In order to assign the same temporal scale to all of them, a signal is send to the PDPA processor. This signal acts as a trigger, setting time 0 for each injection. This time is with respect energizing time.

At the same time, another pulse is sent to the PDPA processor of 6 µs length. This signal controls what is called “Burst Window”, which determines a time window during which bursts can be measured. Droplets detected during pulse duration are measured but, once the pulse finished they are ignored. This procedure allows PDPA system to ignore latter droplets, from the tail of the spray, which are not useful to perform any data analysis.

PDPA RESULTS

DATA PROCESSING

PDA allows measuring the speed and diameter for each Diesel droplet which crosses the area of interest and emits a valid signal. The data is presented as a distribution of velocity and diameter of particles, measured along each injection so it is possible to identify the different states of the Diesel Spray. In Figure 12 is shown the velocity distribution from one of the points tested where are also represented three different zones: Spray arrival, Stabilized Spray and Spray Tail.

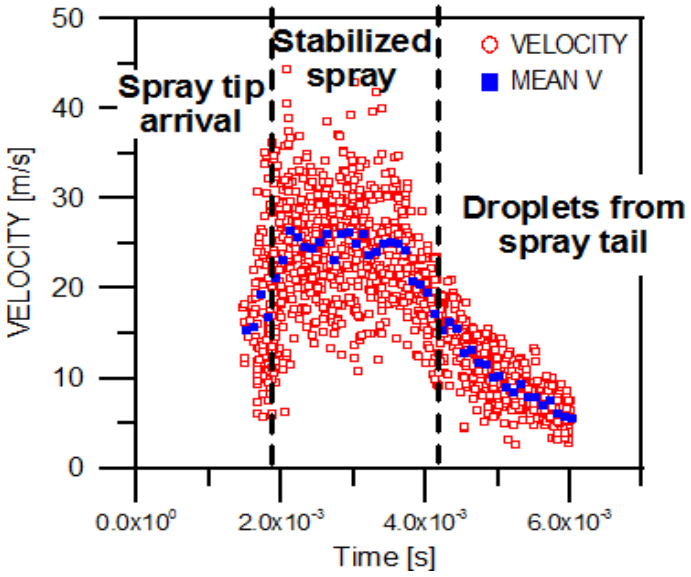

Figure 12. Velocity distribution corresponding to 60 mm on axis from de nozzle, Rail Pressure of 600 bars, charge of 25% and 20kg/m^{3}ambient density.

For the analysis of the influence of the different test parameter on the behavior of the spray, the most interesting data is the one corresponding to droplets measured during the stabilized spray stage. According to this, droplets located at the zones of spray arrival and spray tail are not consider in order to obtain a mean value of velocity and speed from each particular test condition.

Time-defined evolution of the spray is also presented to show variations between the different test conditions. To avoid representing high number of points (red dots in Figure 12) mean Velocity, mean diameter and Sauter mean diameter values were obtained for intervals of 100 µs.

The two different diameter values obtained are considered as atomization indicators. The first one is simpler and more intuitive and it is calculated as a normal mean:

$$\bar{D} = \frac{\sum_{i=1}^{Nd} d_i}{Nd} \qquad (5)$$

The second indicator is de Sauter mean diameter (SMD). It is a very interesting parameter in combustion research because in its mathematical definition the ratio between total liquid volume and the contact surface between this phase and gas is preserved. The correspondent equation is:

$$SMD = \frac{\sum_{i=1}^{Ns} (d_i)^3}{\sum_{i=1}^{Nd} (d_i)^2} \qquad (6)$$

In order to obtain a better comparison between different test points, the time scale for every test has been corrected to make coincident the origin of data with the SOI at each case.

The pulse which triggers the PDPA system measurements for every injection was set up according with the SOI for rail pressure of 600 bar and 22.5% of charge. According to this, the correction was made using the delays between SOE and SOI obtained from Mass Flow measurements and this point as a reference. The next table shows the order of magnitude of corrections made:

Test Conditions	SOI (ms)	DELAY (ms)
600_22.5%	0.3864	0
600_25%	0.3617	-0.0247
600_30%	0.3232	-0.0632
1500_25%	0.4876	0.1012
1500_27.5%	0.4535	0.0671
1500_30%	0.4266	0.0402

Table 4. Delays calculated for different test conditions

PDA Velocity values have to be corrected while the spray axis is not aligned with the measurement axis. In the case of Continental Direct Acting Injector, the spray is deviated 11.68º from measurement X axis.

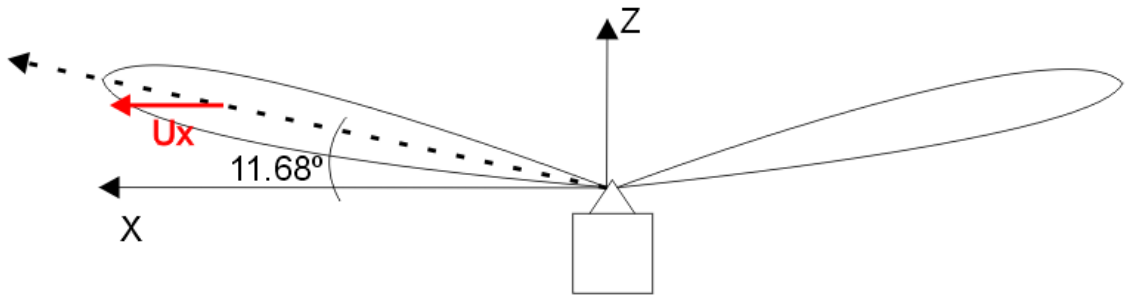

Figure 13. Scheme of the relative position of the spray to the measurement axis

This result of 11.68º is very close to the 12º presented in the Continental drawing of the nozzle. The PDA hardware used at CMT Motores Termicos only has the capability of measuring one velocity.

VELOCITY RESULTS PRESENTATION

In this section all results obtained from measurements of velocity are presented, analyzing the influence of each test parameter. Also, information about difficulties found during measurements will be included.

All velocities represented are values in the axis direction since they have been corrected by the spray included angle.

The results in time domain are corrected with respect time after start of injection, the information obtained from injection rate has been used to correct the delay between start of energizing (acting as trigger) and start of injection that depend the operating point.

VELOCITY MEASUREMENT RESULTS FOR DIFFERENT ON-AXIS LOCATIONS

Mean interval values of velocity obtained at 30, 40, 50 and 60 mm from the nozzle are presented in the following figures.

As you move away from nozzle the droplets reach the measurement volume later. As expected, velocity vs. time curves present a delay between them. Moreover velocities values in the stabilized stage seem to be lower for higher on-axis distances.

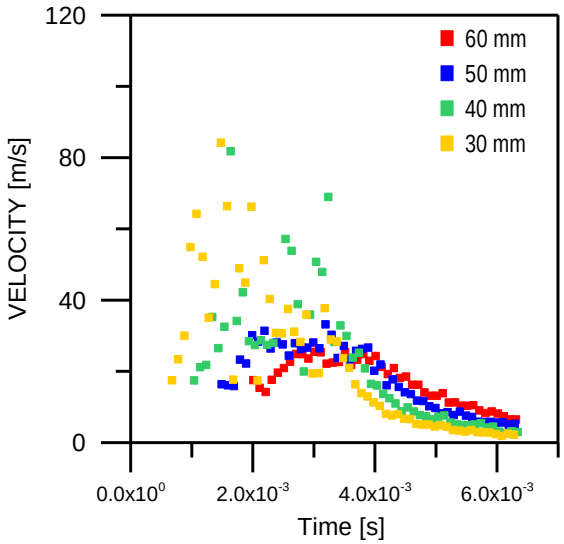

Figure 14. Mean Velocity values at different on-axis positions for Rail Pressure of 600 bar, 20 kg/m^3 ambient density and charge of 22.5%

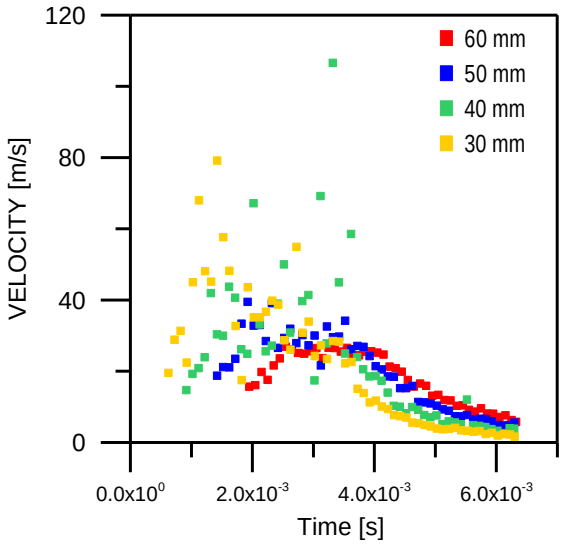

Figure 15. Mean Velocity values at different on-axis positions for Rail Pressure of 600 bar, 20 kg/m^3 ambient density and charge of 25%

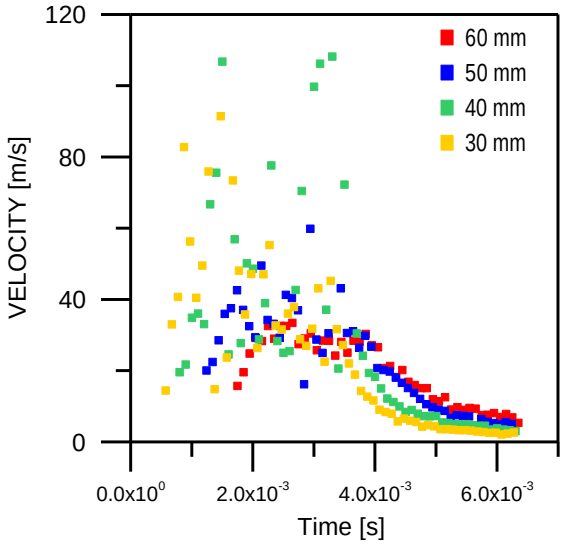

Figure 16. Mean Velocity values at different on-axis positions for Rail Pressure of 600 bar, 20 kg/m^3 ambient density and charge of 30%

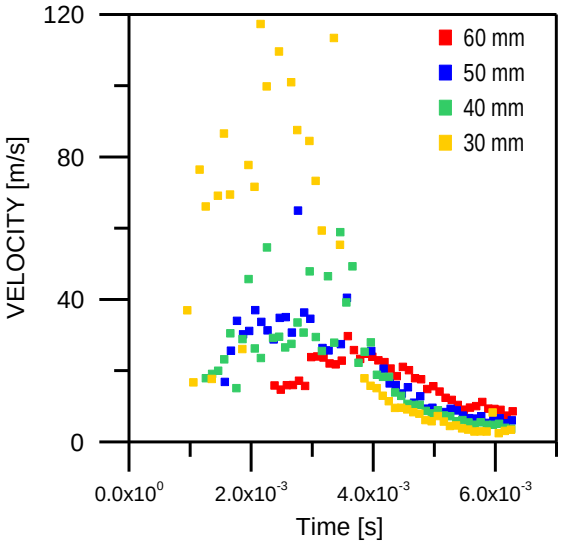

Figure 17. Mean Velocity values at different on-axis positions for Rail Pressure of 1500 bar, 20 kg/m^3 ambient density and charge of 25%

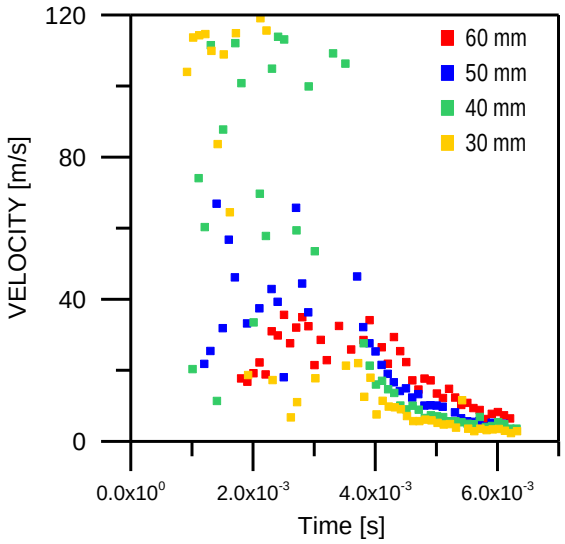

Figure 18. Mean Velocity values at different on-axis positions for Rail Pressure of 1500 bar, 20 kg/m^3 ambient density and charge of 27.5%

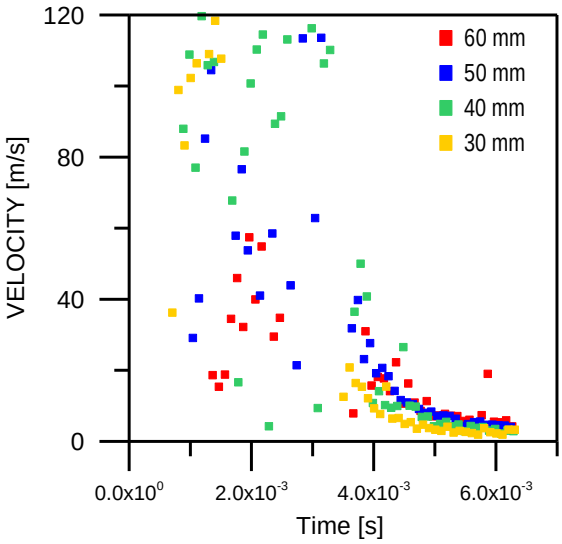

Figure 19. Mean Velocity values at different on-axis positions for Rail Pressure of 1500 bar, 20 kg/m^3 ambient density and charge of 30%

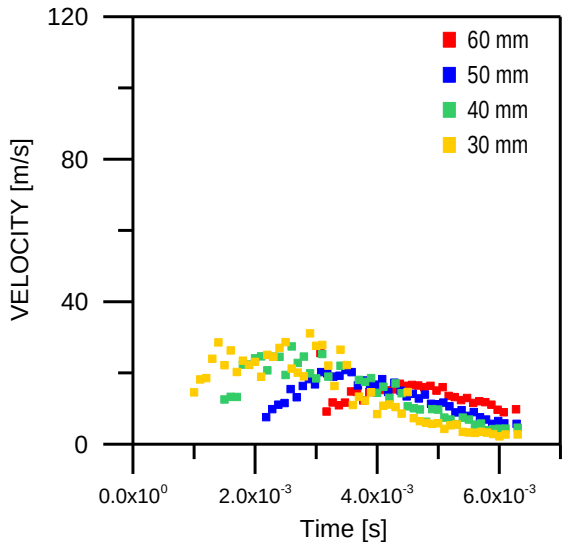

Figure 20. Mean Velocity values at different on-axis positions for Rail Pressure of 1500 bar, 40 kg/m^3 ambient density and charge of 25%

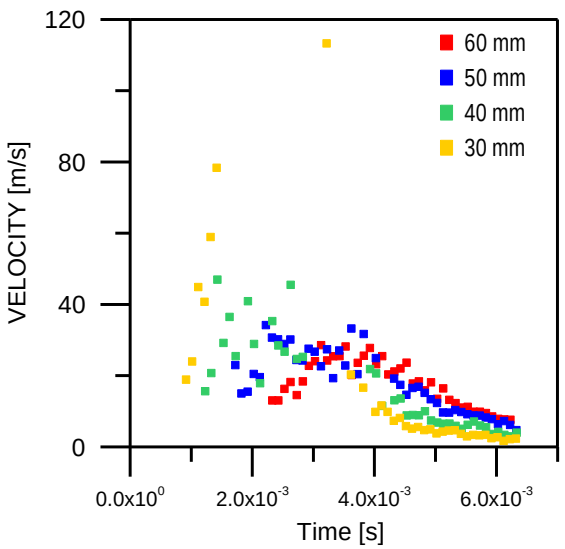

Figure 21. Mean Velocity values at different on-axis positions for Rail Pressure of 1500 bar, 40 kg/m^3 ambient density and charge of 27.5%

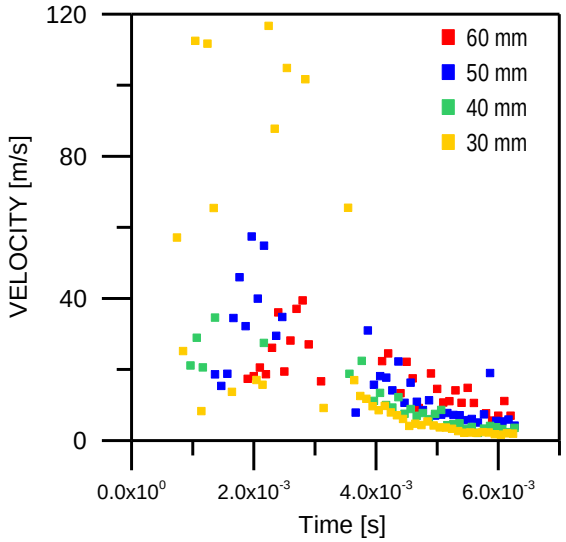

Figure 22. Mean Velocity values at different on-axis positions for Rail Pressure of 1500 bar, 40 kg/m^3 ambient density and charge of 30%

It can be observed that for test conditions which imply higher droplet velocities (high rail pressure, low ambient density and high piezo charges) quality of measurements is worst, which is clearly appreciable in Figure 19. This can be related to the fact that faster droplets are difficult to detect and measure for the PDA system. For points near the injector nozzle this is also appreciable and it can be justified due to the high droplet density at this positions. This fact is one of the reasons why points nearer the nozzle were not included in the test plan.

VELOCITY AVERAGE VALUES FOR DIFFERENT ON-AXIS POSITIONS

The following figures represent the mean velocity value for the stabilized spray zone at each test point. These values are presented with its corresponding confidence interval.

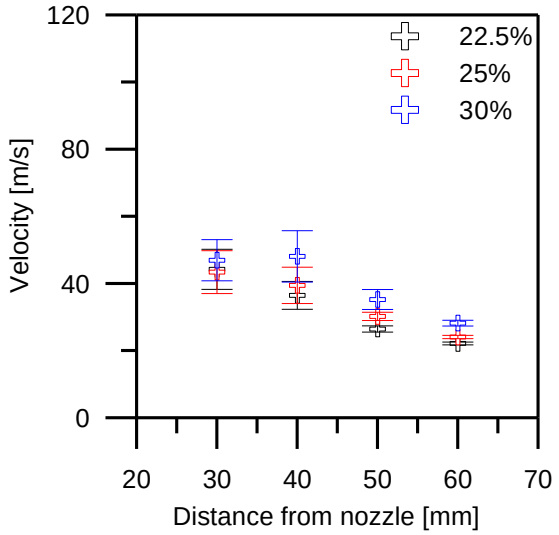

Figure 23. Mean velocity values at stabilized spray zone for Rail Pressure of 600 bar and 20 kg/m^3 ambient density

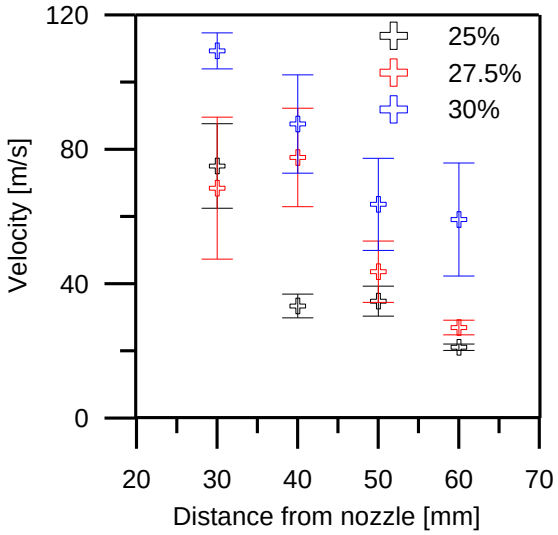

Figure 24. Mean velocity values at stabilized spray zone for Rail Pressure of 1500 bar and 20 kg/m^3 ambient density

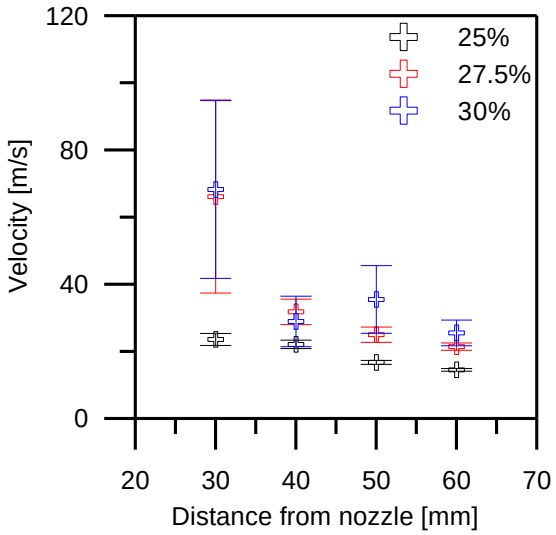

Figure 25. Mean velocity values at stabilized spray zone for Rail Pressure of 1500 bar and 40 kg/m^3 ambient density

In these figures the velocity trend commented in the upper lines can be observed. High Rail Pressure, low ambient density and high charge percentage represent higher droplet velocity. It is important to highlight that these values are related very closely with the quality of the data. It can be seen that the confident interval size increases with the velocity value. This is due to the measurement difficulties analyzed before and can lead to wrong estimations.

VELOCITY MEASUREMENT RESULTS FOR DIFFERENT RADIAL LOCATIONS

The analysis of radial distribution of particles is interesting in order to characterize not only the jet axis but also the whole section of it. This is why different radial positions at 40 and 50 mm on the axis were included in the test plan. The figures presented below show mean velocity values at 4 radial positions of the section at 40 mm on the spray axis.

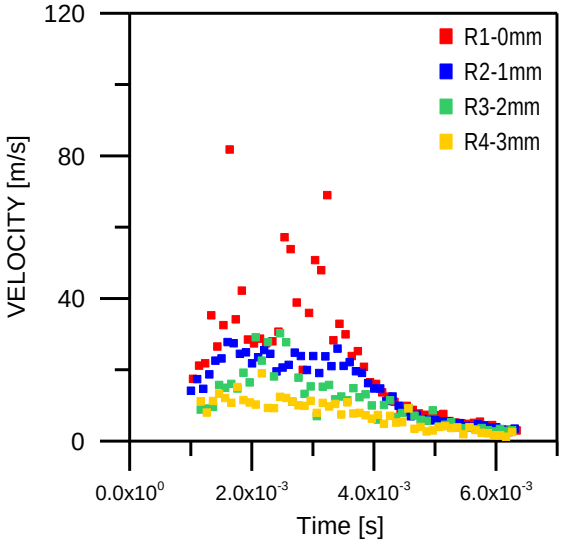

Figure 26. Mean velocity values at different radial positions for Rail Pressure of 600 bar, 20 kg/m^3 ambient density and charge of 22.5%

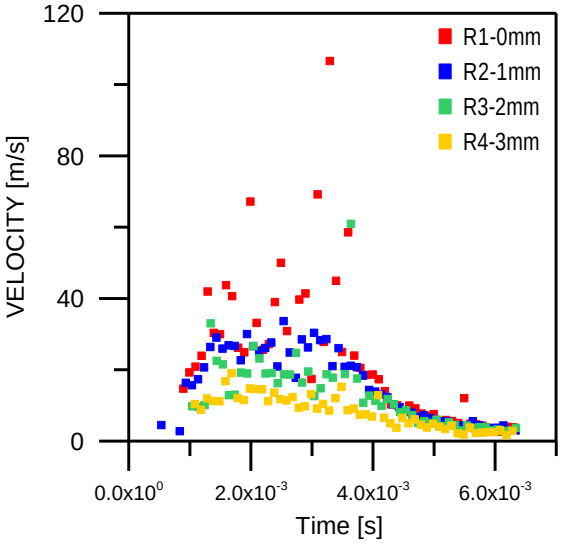

Figure 27. Mean velocity values at different radial positions for Rail Pressure of 600 bar, 20 kg/m^3 ambient density and charge of 25%

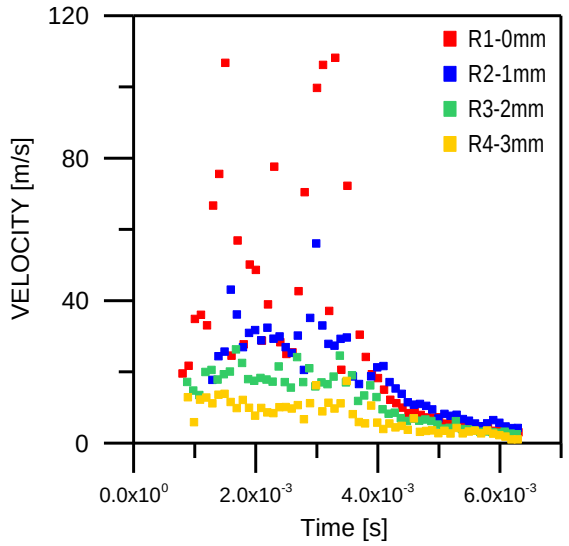

Figure 28. Mean velocity values at different radial positions for Rail Pressure of 600 bar, 20 kg/m^3 ambient density and charge of 30%

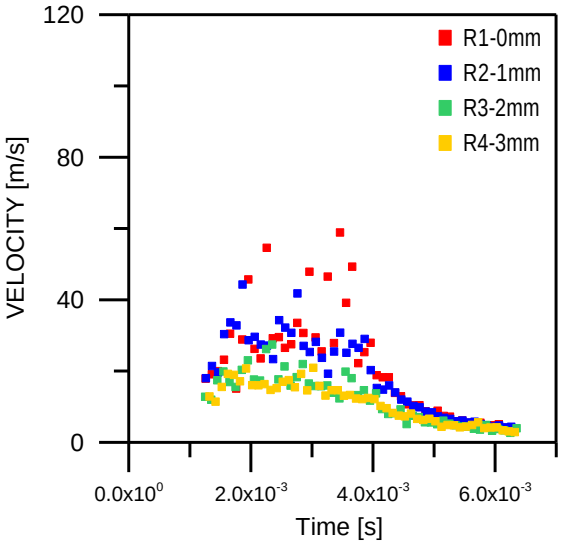

Figure 29. Mean velocity values at different radial positions for Rail Pressure of 1500 bar, 20 kg/m^3 ambient density and charge of 25%

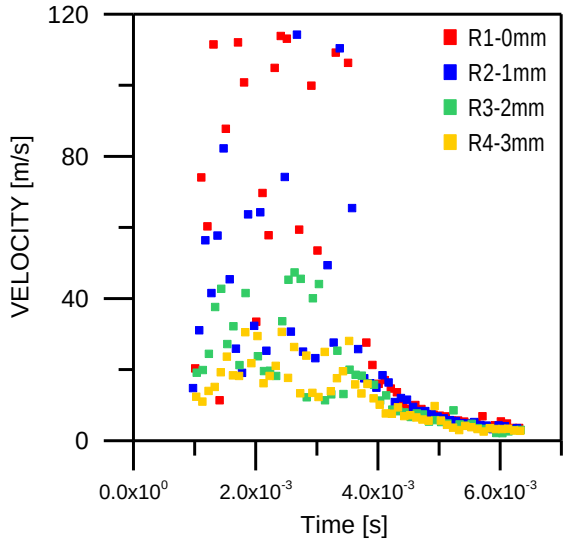

Figure 30. Mean velocity values at different radial positions for Rail Pressure of 1500 bar, 20 kg/m^3 ambient density and charge of 27.5%

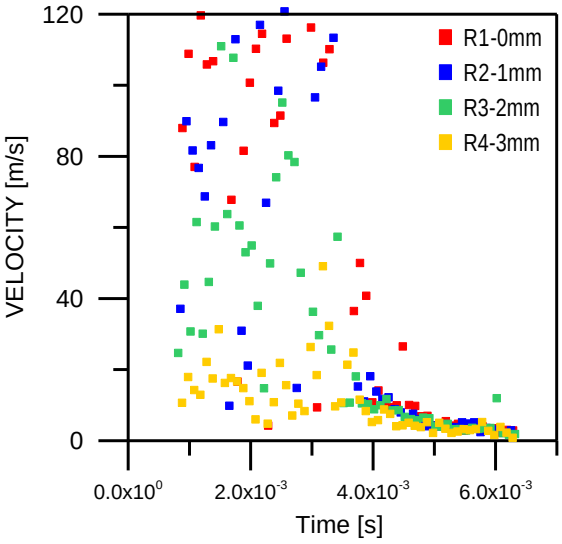

Figure 31. Mean velocity values at different radial positions for Rail Pressure of 1500 bar, 20 kg/m^3 ambient density and charge of 30%

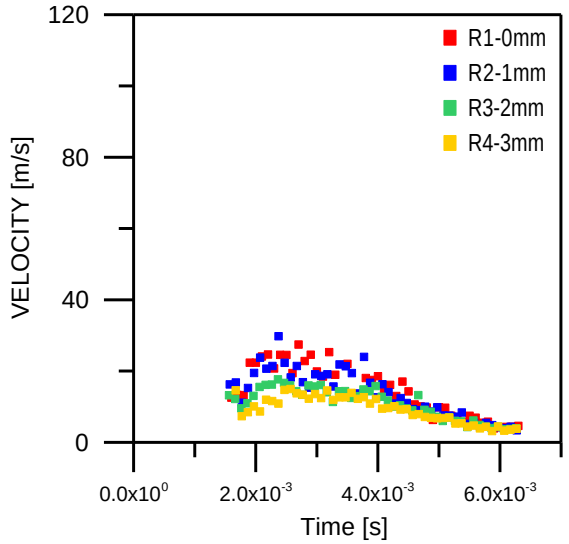

Figure 32. . Mean velocity values at different radial positions for Rail Pressure of 1500 bar, 40 kg/m^3 ambient density and charge of 25%

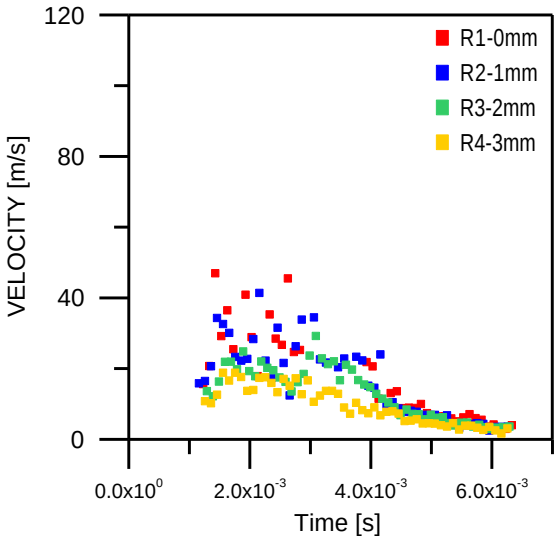

Figure 33. Mean velocity values at different radial positions for Rail Pressure of 1500 bar, 40 kg/m^3 ambient density and charge of 27.5%

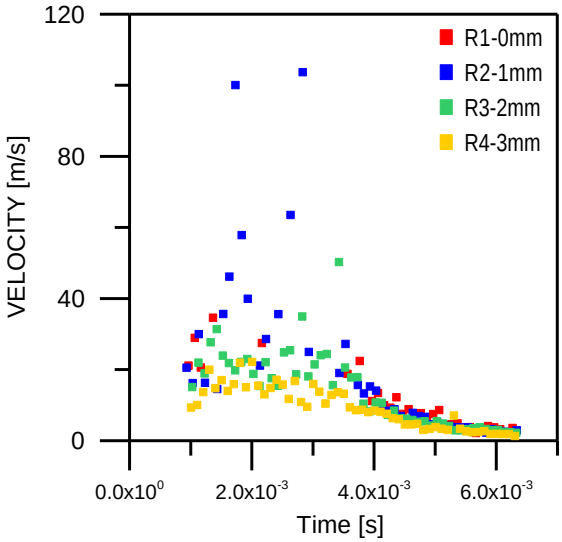

Figure 34. Mean velocity values at different radial positions for Rail Pressure of 1500 bar, 40 kg/m^3 ambient density and charge of 30%

The previous figures show a big influence of the charge on droplets near spray axis. However the charge variation do not affect significantly droplets velocity far from the axis as can be observed, comparing Figure 26, Figure 27 and Figure 28.

The Figure 35 shows the evolution regarding the distance to the axis of the amount of measured droplets of the spray stabilized stage. As expected, the number of measured droplets increase as the position gets farther from the axis (increasing radial distance). This is due to a lower mean droplet velocity value and also a lower droplet concentration of them that enables PDA system to detect and measure a bigger quantity of particles.

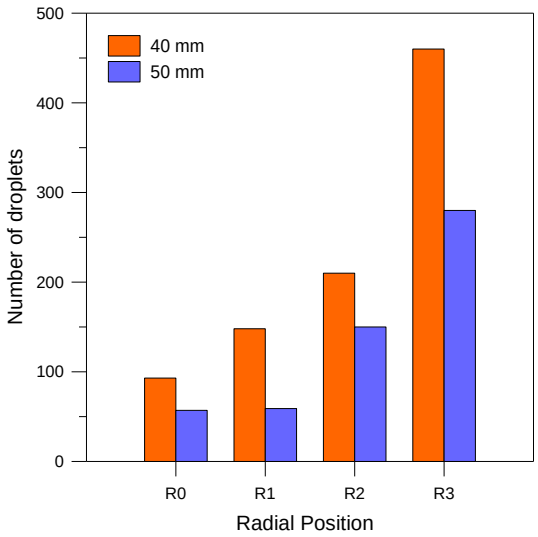

Figure 35. Bar chart of the number of droplets measured at different radial positions for 40 and 50 mm sections with a rail pressure of 1500 bar, 20 kg/m^3 ambient density and 25% charge.

VELOCITY AVERAGE VALUES FOR DIFFERENT RADIAL LOCATIONS

The following figures present mean velocity values of the stabilized spray stage for the 4 different radial positions at a section located 40 mm from nozzle. It is included also the confidence interval for every mean value.

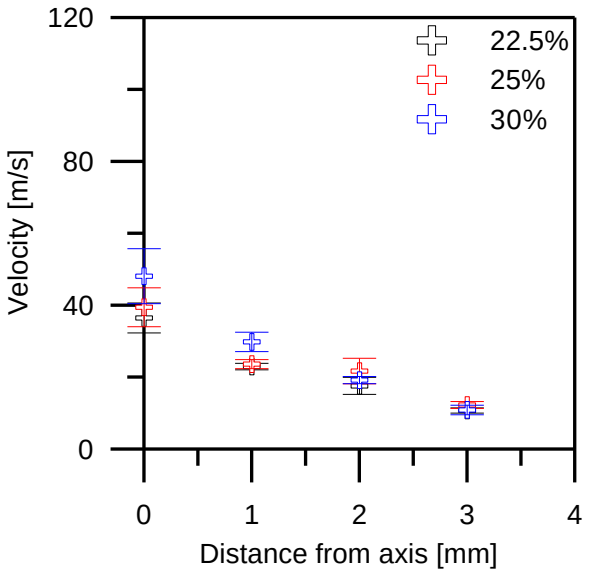

Figure 36. Mean velocity values at stabilized spray zone for Rail Pressure of 600 bar and 20 kg/m^3 ambient density

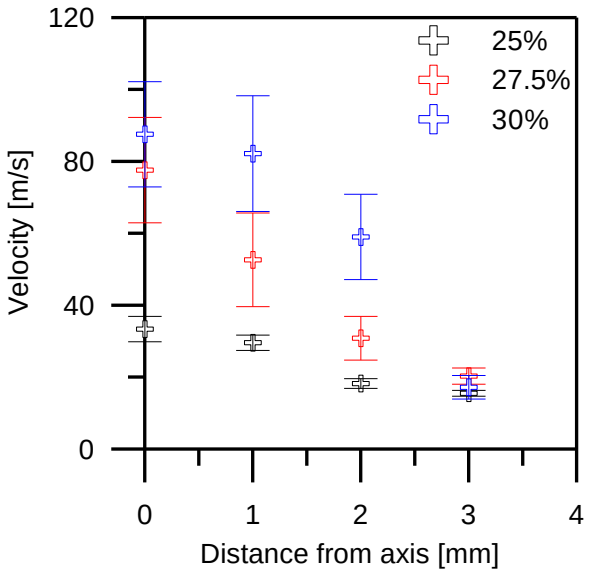

Figure 37. Mean velocity values at stabilized spray zone for Rail Pressure of 1500 bar and 20 kg/m^3 ambient density

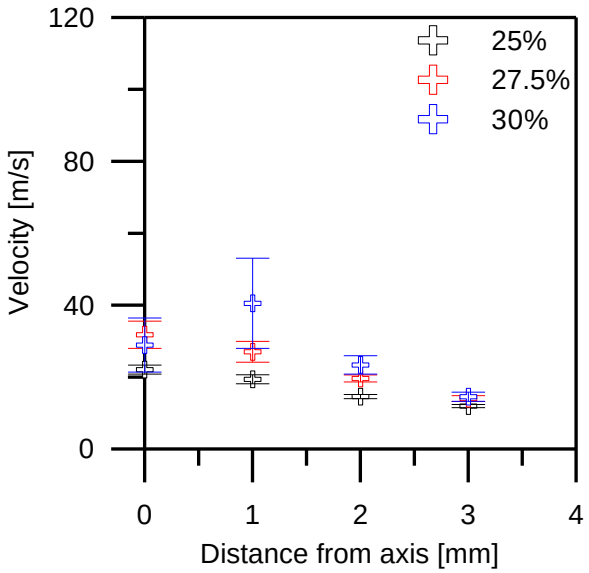

Figure 38. Mean velocity values at stabilized spray zone for Rail Pressure of 1500 bar and 40 kg/m^3 ambient density

As expected, the mean velocity values decrease with the distance to the spray axis. This figures also confirm that the increase of the charge do not affect all the radial position velocities in the same way. In Figure 37 can be noticed this fact, showing that there are almost no differences between the three charge conditions at 3 mm from the axis. On the other hand, the opposite can be observed for near axis positions.

The measurements at 50 mm from the nozzle are not presented because they show the same trends as measurements at 40 mm. In the Figure 39 this can be observed, comparing several velocity mean values at the two different sections.

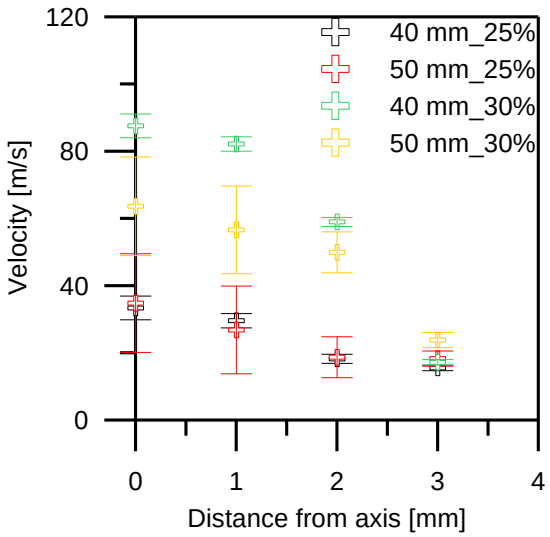

Figure 39. Mean velocity values at stabilized spray zone for Rail pressure of 1500 bar and 20kg/m^3 ambient density.

VELOCITY MEASUREMENT RESULTS FOR DIFFERENT RAIL PRESSURES

Rail pressure is directly related to droplet velocity and can cause variations in the geometry of the spray. The effects of this parameter are well known but together with the variable charge of this injector generate a new problem to analyze.

In the following figures evolution of mean velocity values is presented comparing rail pressures at different axis positions in combination with two injector charge values.

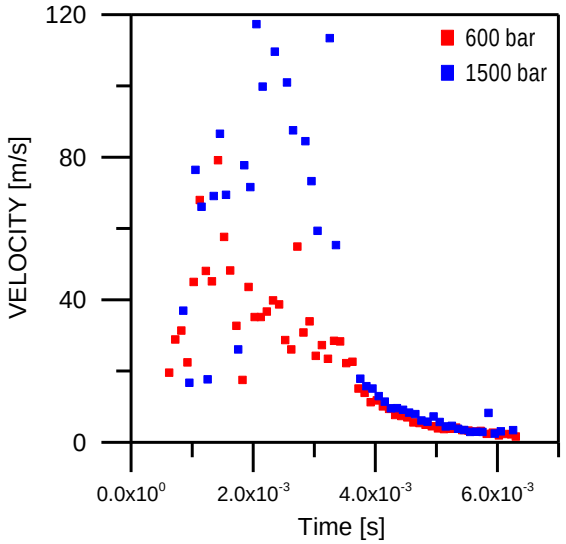

Figure 40. Mean velocity values for 20kg/m^3 ambient density, at 30 mm from nozzle and charge of 25%

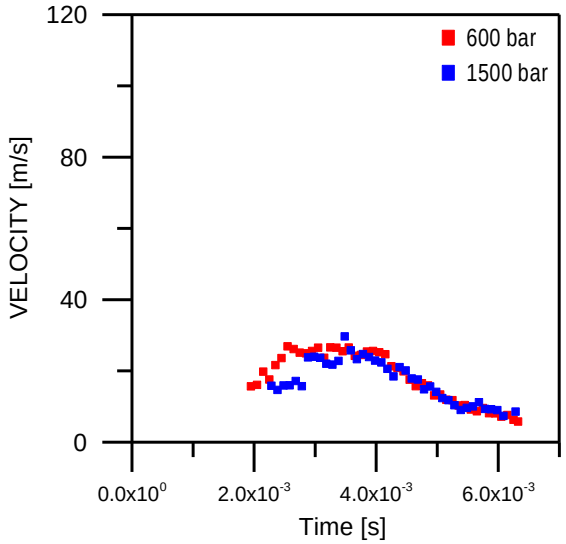

Figure 41. Mean velocity values for 20kg/m^3 ambient density, at 60 mm from nozzle and charge of 25%

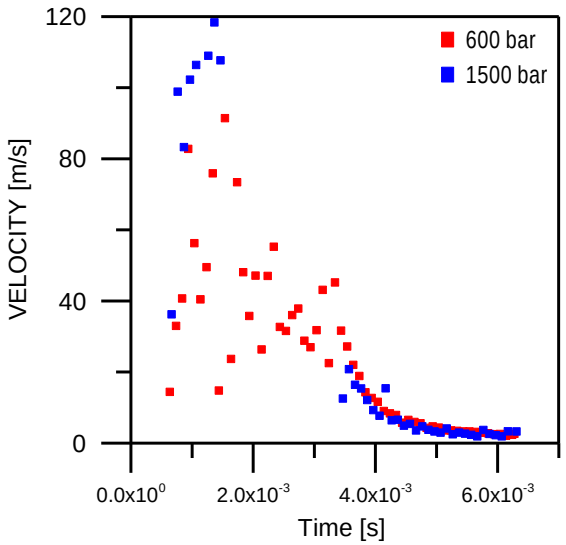

Figure 42. Mean velocity values for 20kg/m^3 ambient density, at 30 mm from nozzle and charge of 30%

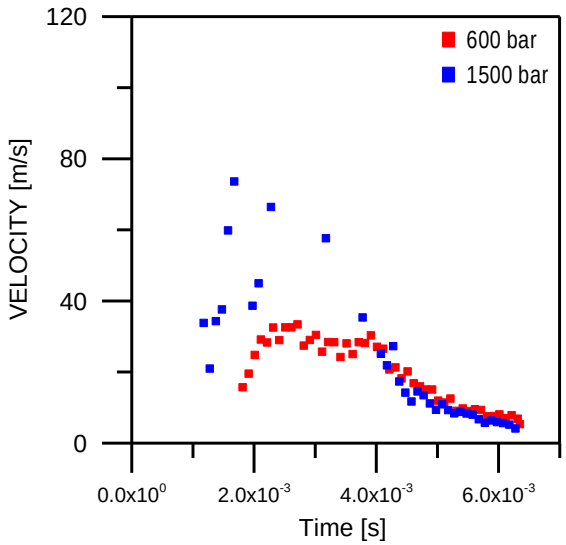

Figure 43. Mean velocity values for 20kg/m^3 ambient density, at 60 mm from nozzle and charge of 30%

In these figures it can be observed:

- For higher injection pressures, the spray arrives to the test volume earlier. This is consistent with the fact that droplet velocities are supposed to increase with the rail pressure.
- The combination with high charge emphasizes the differences on droplet velocity values between high and low rail pressure measurements.
- Measurement presented at Figure 42 for high pressure show low quality results (low quantity of droplets measured at stabilized zone) due to the difficulty of measuring near the nozzle, with high droplet velocities and density.

In order to visualize clearly the effect of rail pressure and charge on axis position the next figures are included.

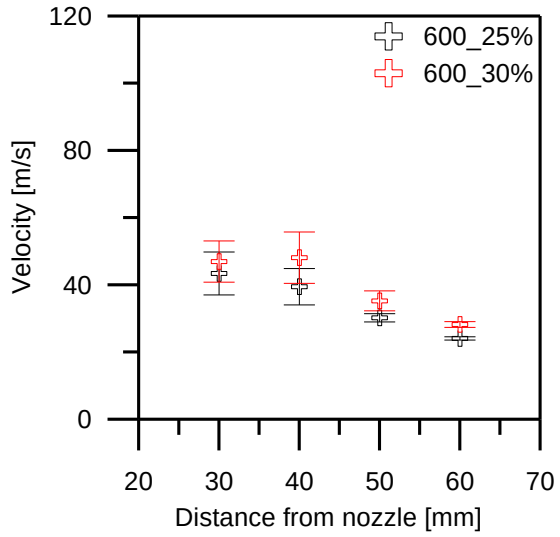

Figure 44. Mean velocity values at stabilized spray zone for 600 bar rail pressure and 20 kg/m^3 ambient density

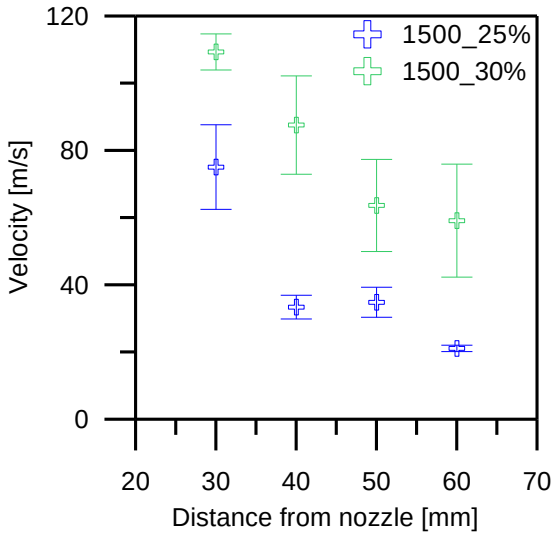

Figure 45. Mean velocity values at stabilized spray zone for 1500 bar rail pressure and 20 kg/m^3 ambient density

Comparing both figures it can be observed that the conclusions taken in the analysis of the first figures is consistent. On one hand, higher rail pressure implies higher droplet velocity at the whole axis. On the other hand, the influence of charge on velocity is more important for higher rail pressure values.

The same analysis as before can be done for different radial positions at 50 mm from nozzle. Some figures are presented below to show the influence of rail pressure in combination with injector charge on the spray section.

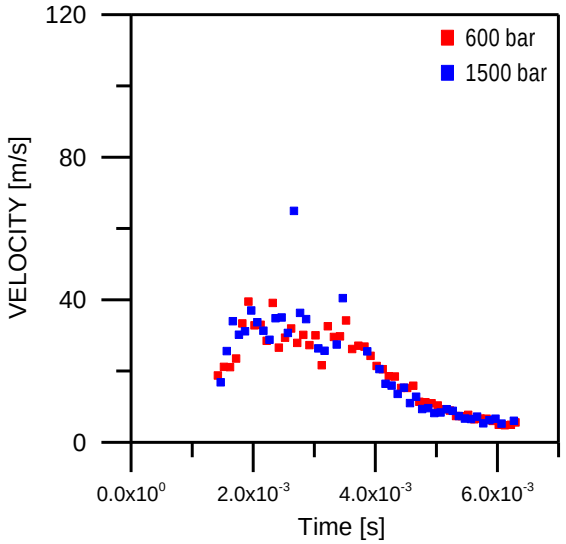

Figure 46. Mean velocity values for 20kg/m^3 ambient density at 50 mm from nozzle, on axis and 25% charge

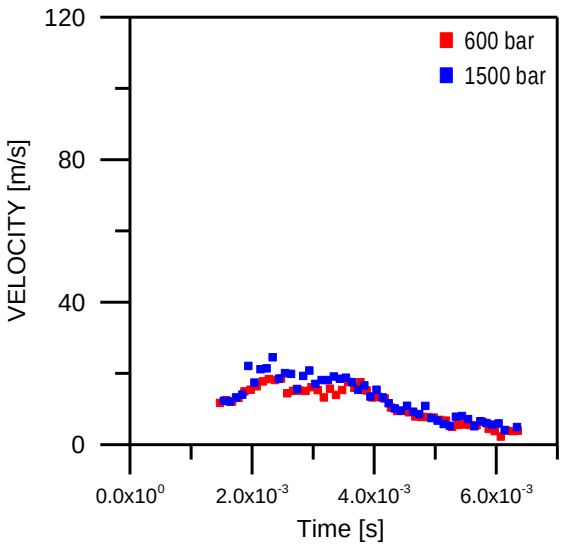

Figure 47. Mean velocity values for 20kg/m^3 ambient density at 50 mm from nozzle, 3 mm from axis and 25% charge

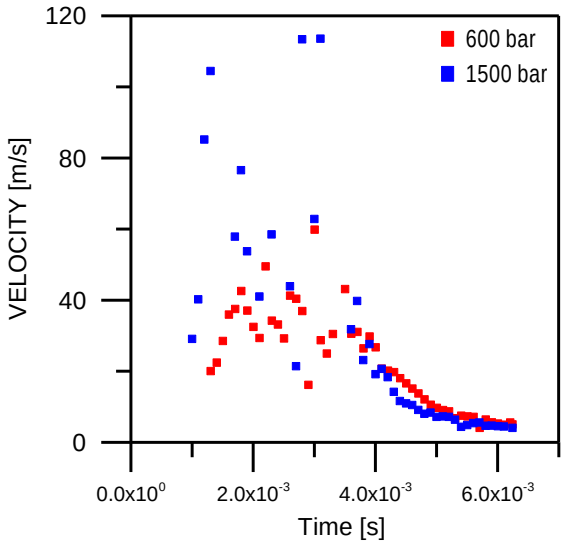

Figure 48. Mean velocity values for 20kg/m^3 ambient density at 50 mm from nozzle, on axis and 30% charge

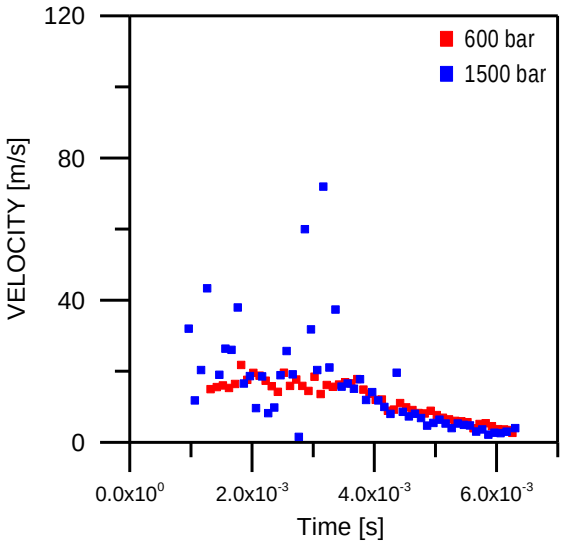

Figure 49. Mean velocity values for 20kg/m^3 ambient density at 50 mm from nozzle, 3 mm from axis and 30% charge

As expected, higher rail pressure implies higher velocities on both positions. However, this effect is more noticeable on axis than at 3 mm away from it. It can be observed that for higher values of charge the influence of pressure is bigger.

The influence of charge on the effect of rail pressure at the sprat section is better represented in the following figures. Mean velocity values at stabilized spray zone are presented to show how the combination of these two parameters affect the behavior of the spray.

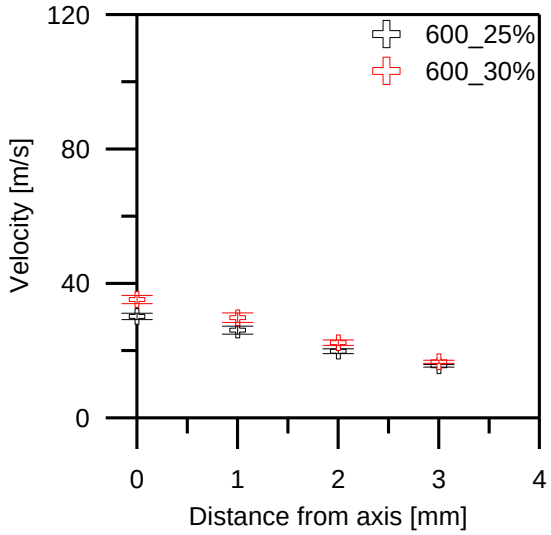

Figure 50. Mean velocity values at stabilized spray zone for 600 bar rail pressure and 20 kg/m^3 ambient density, at different distances from axis

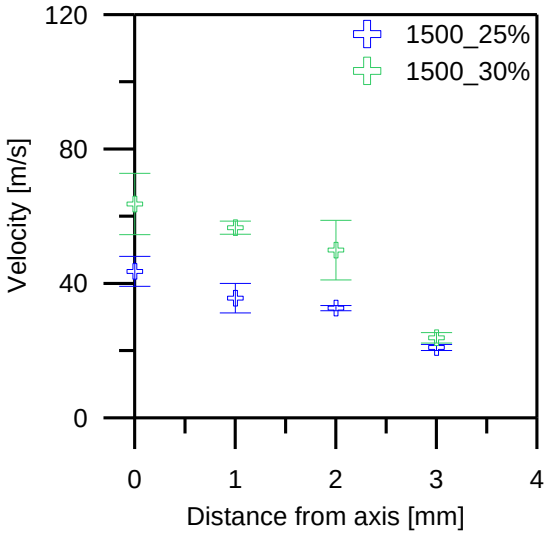

Figure 51. Mean velocity values at stabilized spray zone for 1500 bar rail pressure and 20 kg/m^3 ambient density, at different distances form axis

In Figure 50 it is shown that with lower rail pressures (600 bar) the influence of charge is not noticeable. However, for higher rail pressures (1500 bar) droplet velocity values are noticeable different between the two injector charge cases. It can be observed that this effect decreases as long as the radial distance from the axis increases (arriving near the spray edge).

VELOCITY MEASUREMENT RESULTS FOR DIFFERENT DENSITY VALUES

The increasing of ambient density implies a further slowdown of the spray which means lower droplet velocities at each test position. The figures included below show the differences between positions along the axis and the combination with different charge values.

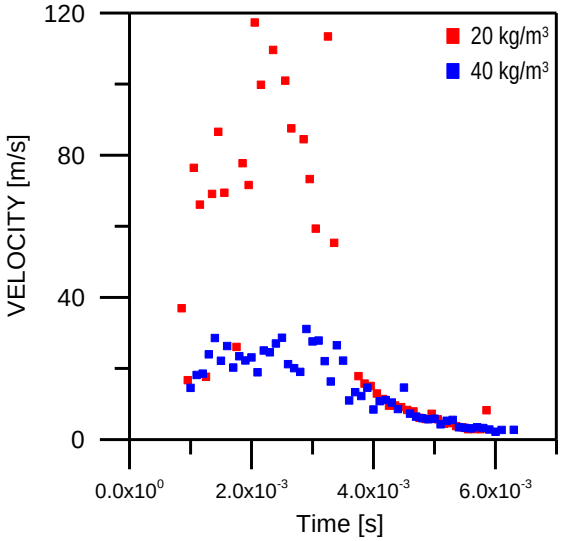

Figure 52. Mean velocity values for rail pressure of 1500 bar, at 30 mm from nozzle on axis and 25% charge

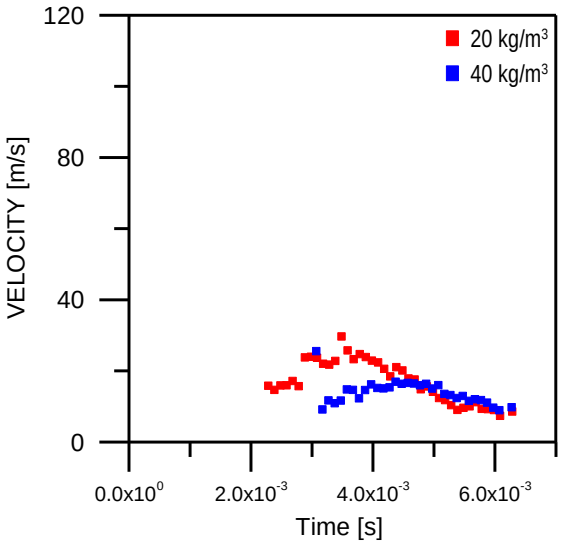

Figure 53. Mean velocity values for rail pressure of 1500 bar, at 60 mm from nozzle on axis and 25% charge

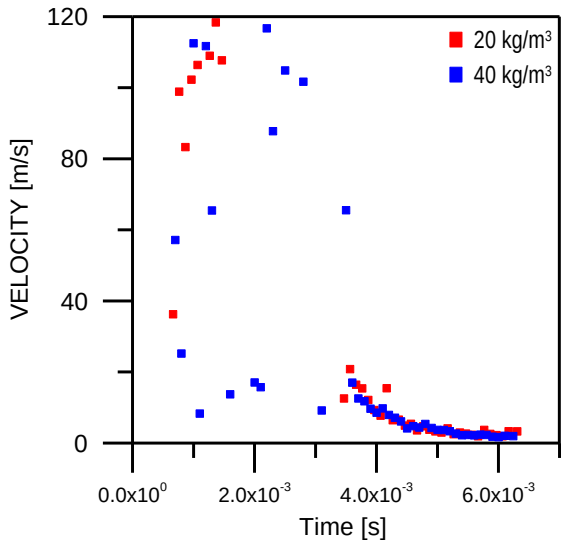

Figure 54. Mean velocity values for rail pressure of 1500 bar, at 30 mm from nozzle on axis and 30% charge

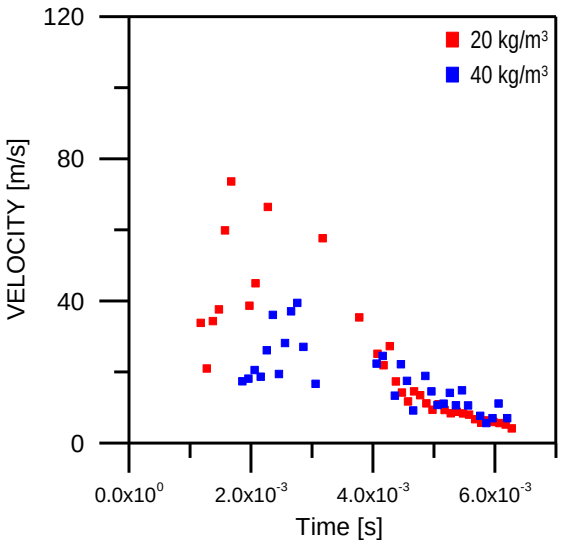

Figure 55. Mean velocity values for rail pressure of 1500 bar, at 60 mm from nozzle on axis and 30% charge

Figure 53 clearly shows the consequence of a higher ambient density. For the same injection conditions, the spray arrives later to 60 mm from nozzle as it is represented by the existent delay between the first droplets measured with 20 kg/m3 and the same with 40 kg/m3. In agreement with this, velocity values obtained are lower for higher ambient densities.

For near to nozzle positions, it seems that higher injector charges countervail the increase of ambient density obtaining velocity values similar to lower ambient densities (Figure 54). However this effect is less significant for points far from the nozzle (Figure 55).

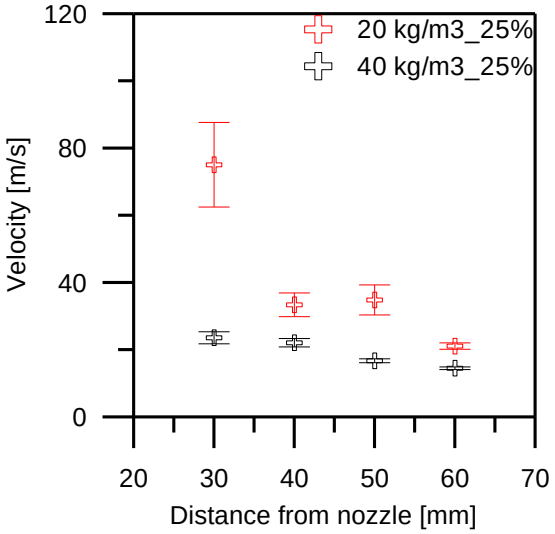

Figure 56. Mean velocity values at stabilized spray zone for 1500 bar rail pressure and 25% charge, at different distances from axis

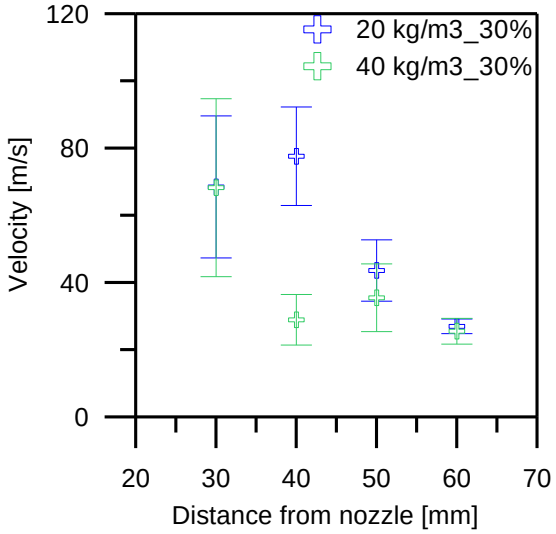

Figure 57. Mean velocity values at stabilized spray zone for 1500 bar rail pressure and 30% charge, at different distances from axis

Figure 56 confirms that the effect of the charge, in combination with ambient density variations, on droplet velocities is more important at 30 mm from nozzle than at 60 mm.

The same analysis made along the axis can be made for the section of the spray. Several figures from a section at 50 mm from the nozzle are represented.

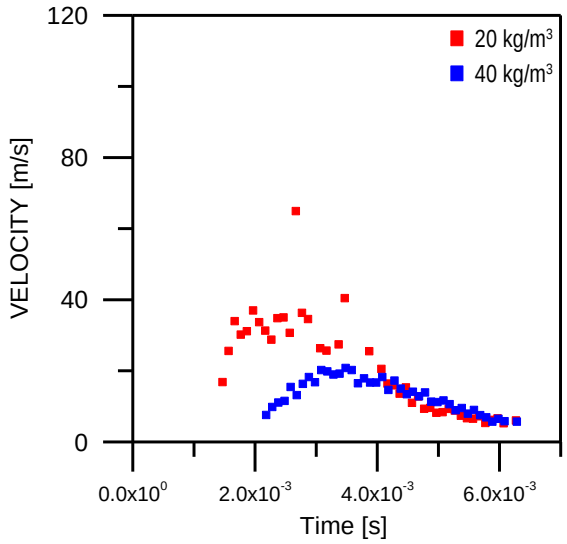

Figure 58. Mean velocity values for rail pressure of 1500 bar, at 50 mm from nozzle on axis and 25% charge

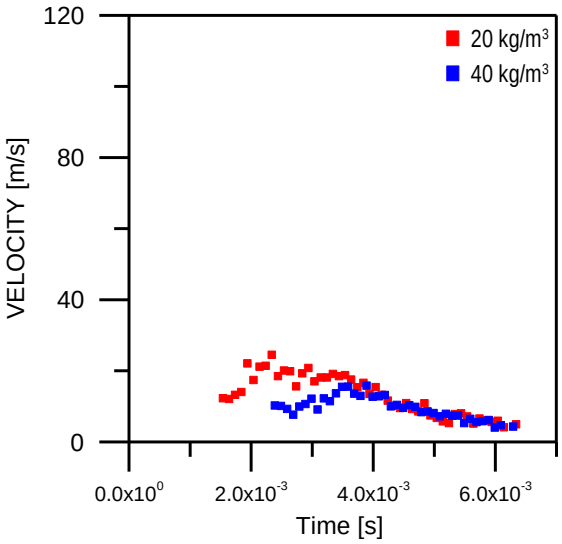

Figure 59. Mean velocity values for radial pressure of 1500 bar, at 50 mm from nozzle, 3 mm from axis and 25% charge

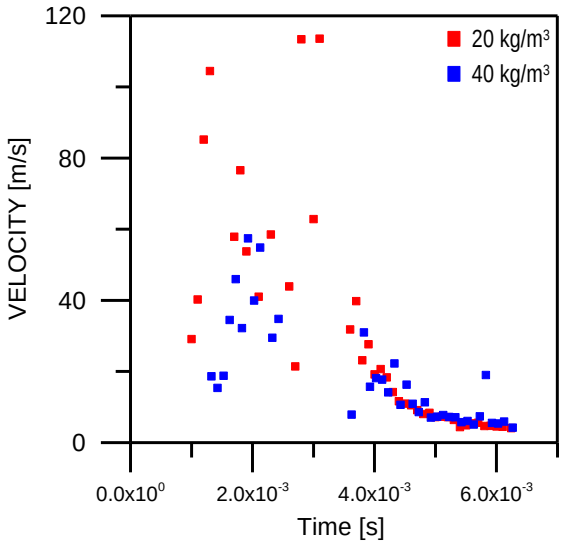

Figure 60. Mean velocity values for rail pressure of 1500 bar, at 50 mm from nozzle on axis and 30% charge

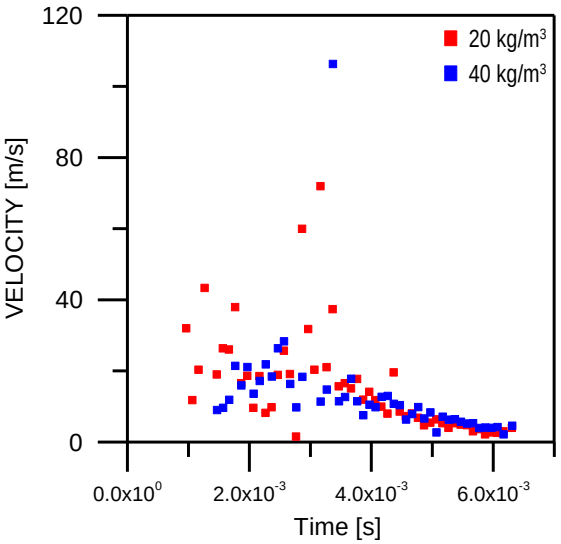

Figure 61. Mean velocity values for radial pressure of 1500 bar, at 50 mm from nozzle, 3 mm from axis and 30% charge

With low ambient density, differences between droplet velocity on axis and at 3 mm away from it are higher than with high ambient density. The effect of the charge increase seems to be similar in the whole section.

For a further analysis of the effects of ambient density variations on spray section the mean values at stabilized spray zone for different radial positions are presented below.

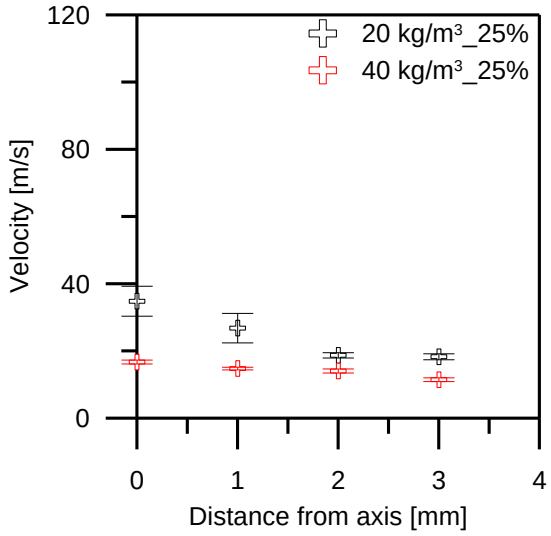

Figure 62. Mean velocity values at stabilized spray zone for 1500 bar rail pressure and 25% charge, at different distances from axis

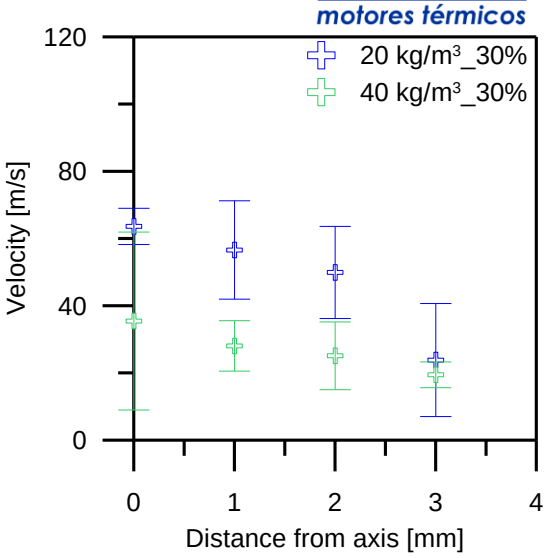

Figure 63. Mean velocity values at stabilized spray zone for 1500 bar rail pressure and 30% charge, at different distances from axis

It can be observed that for high ambient density the velocity profile across the spray section has fewer slopes than for lower ambient density. In other words, velocity values are very similar between on-axis and off-center positions in a same section. This velocity profile, however, increases its slope for higher charge values.

DIAMETER RESULTS PRESENTATION

In this section, droplet diameter results will be presented analyzing the influence of every test parameter and their combination with different injector charge values.

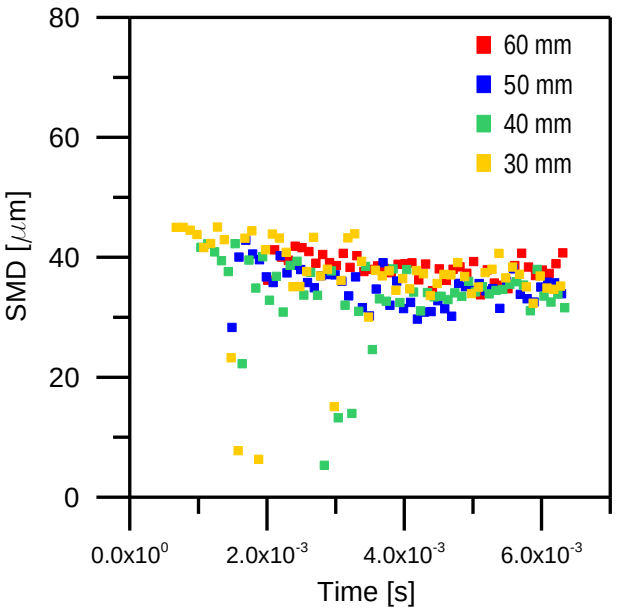

Figure 64. Mean diameter values for rail pressure of 600 bar, 20 kg/m^3 ambient density and 22.5% charge

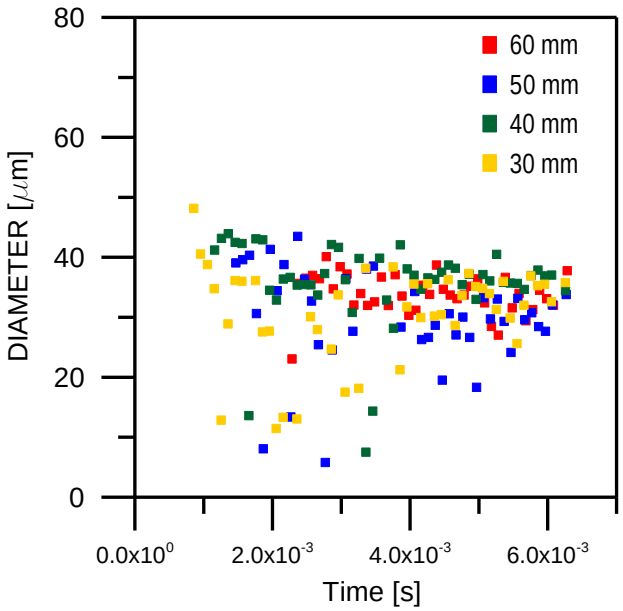

Figure 65. Mean diameter values for rail pressure of 1500 bar, 20 kg/m^3 ambient density and 25% charge

A typical result of diameter measurements is shown in Figure 64 and Figure 65. It can be seen that the mean value does not vary too much along the time test window, so it was considered that time resolution in this case is not necessary. According to this, from now on only Sauter mean diameter and average diameter values from stabilized spray zone will be used in the analysis.

However is important to remark that, caused by the uncertainties of PDPA, tests present dispersion at diameter measurements which could affect mean values. Analysis has to be done very carefully in order to detect this kind of problem and if it affects the final results.

DIAMETER MEASUREMENT RESULTS FOR DIFFERENT RADIAL AND ON-AXIS LOCATIONS

Mean diameter and Sauter mean diameter values at stabilized spray stage were calculated at every position defined for the test plan. This allows obtaining and representing the evolution of these parameters, not only along the axis but also over the spray section.

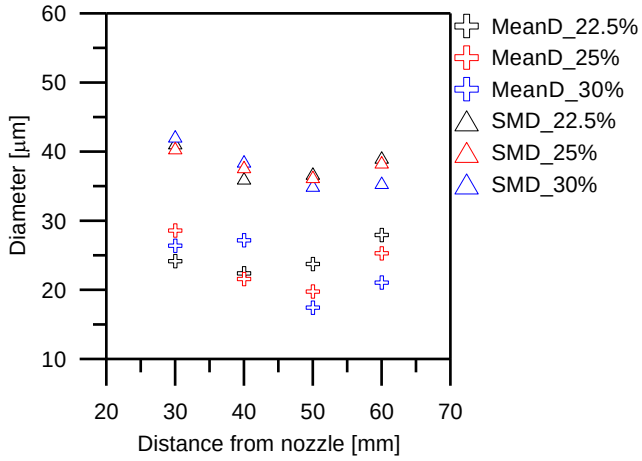

Figure 66. Mean and Sauter mean diameter values at stabilized spray zone for 600 bar rail pressure, 20 kg/m^3 ambient density, at different distances from nozzle

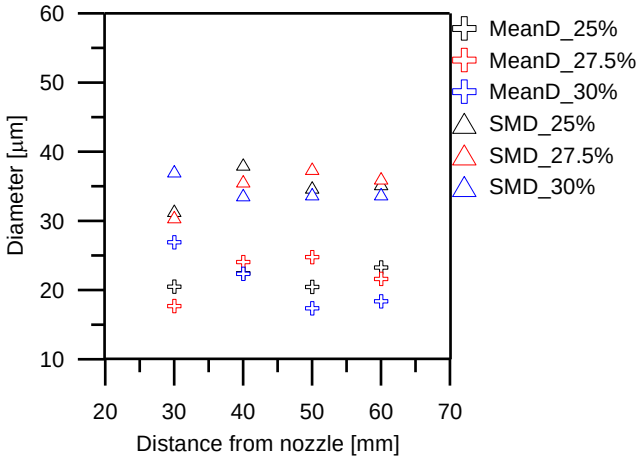

Figure 67. Mean and Sauter mean diameter values at stabilized spray zone for 1500 bar rail pressure, 20 kg/m^3 ambient density, at different distances from nozzle

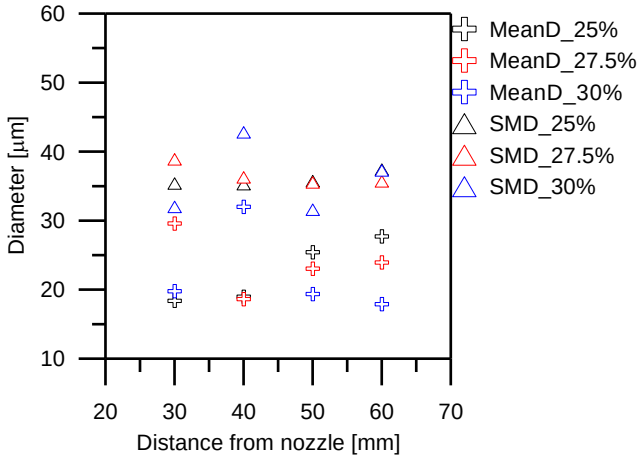

Figure 68. . Mean and Sauter mean diameter values at stabilized spray zone for 1500 bar rail pressure, 40 kg/m^3 ambient density, at different distances from nozzle

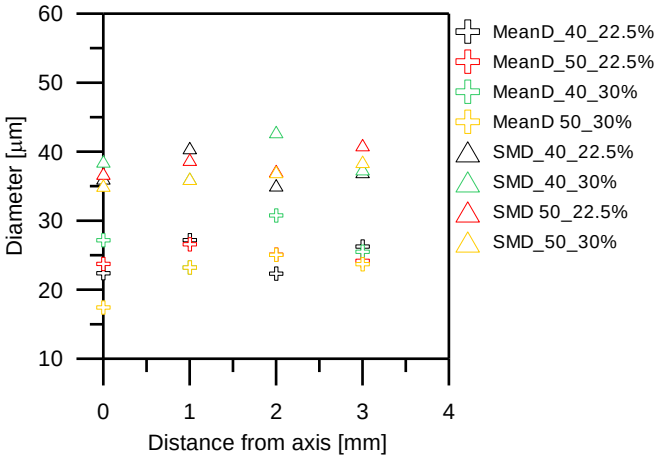

Figure 69. Mean and Sauter mean diameter values at stabilized spray zone for 600 bar rail pressure, 20 kg/m^3 ambient density, at different distances from axis

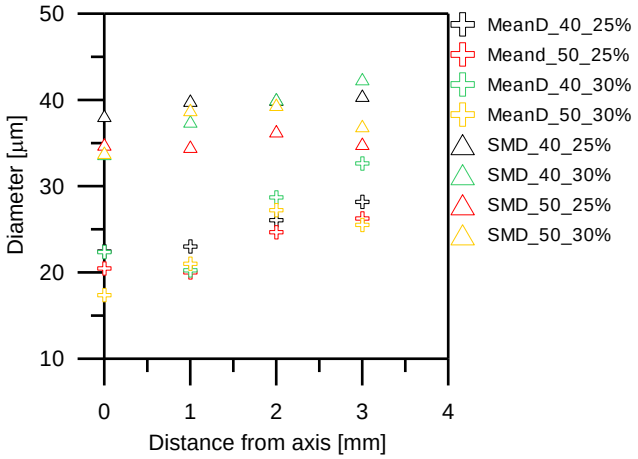

Figure 70. Mean and Sauter mean diameter values at stabilized spray zone for 1500 bar rail pressure, 20 kg/m^3 ambient density, at different distances from axis

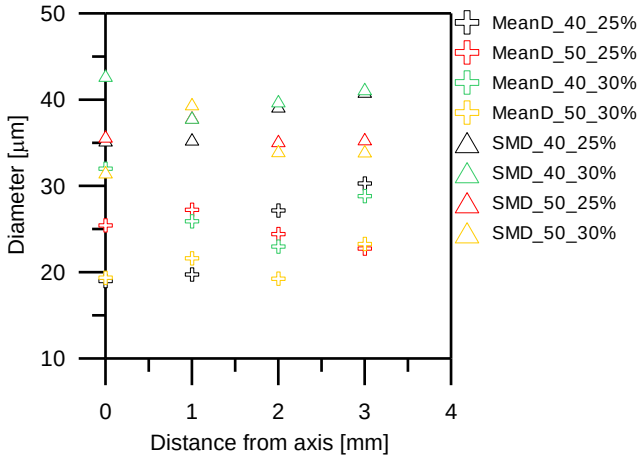

Figure 71. Mean and Sauter mean diameter values at stabilized spray zone for 1500 bar rail pressure, 40 kg/m^3 ambient density, at different distances from axis

It can be observed on all the figures that there is no clear trend represented, neither for spatial evolution nor charge influence. However, it seems (Figure 67) that diameter goes down as droplets advance but this is not actually consistent with what is found in the literature. Moreover, in Figure 70 data shows an increase of droplets diameter with distance from the axis.

In the side of charge, it is supposed that an increase of this parameter implies a reduction of the droplet diameter. This trend can be appreciated at Figure 66 for SMD but in the rest of them is difficult to affirm the same. So in this case no conclusion about charge influence can be drawn.

DIAMETER MEASUREMENT RESULTS FOR DIFFERENT RAIL PRESSURES AND AMBIENT DENSITIES

Injection pressure and ambient density are related with the atomization mechanisms, which controls the final droplet diameter at the spray and its evolution. In order to find

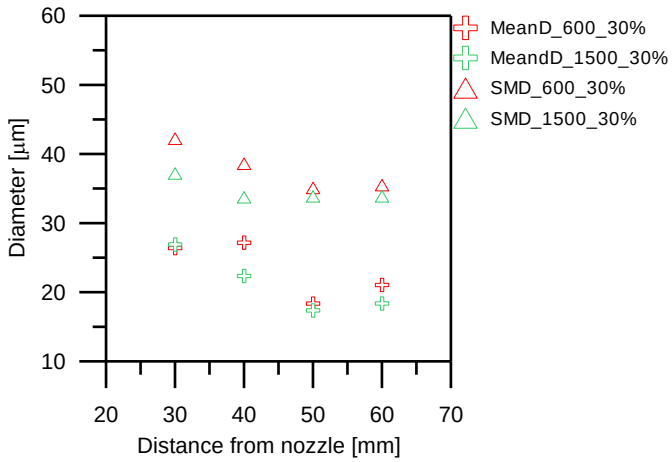

Figure 72. Mean and Sauter mean diameter values at stabilized spray zone for 20 kg/m^3 ambient density, at different distances from nozzle

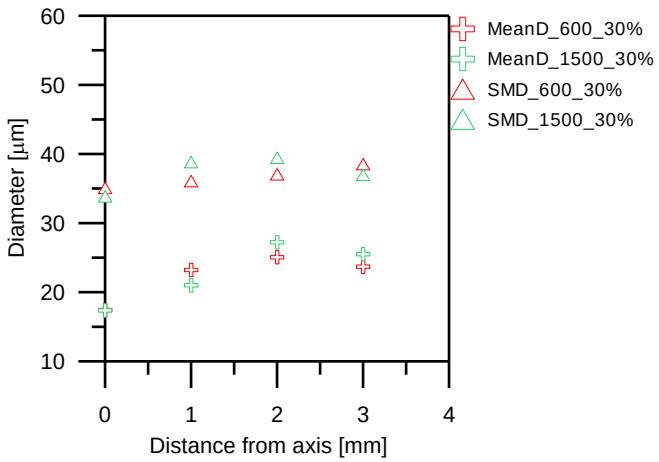

Figure 73. Mean and Sauter mean diameter values at stabilized spray zone for 20 kg/m^3 ambient density, 50 mm from nozzle at different distances from axis

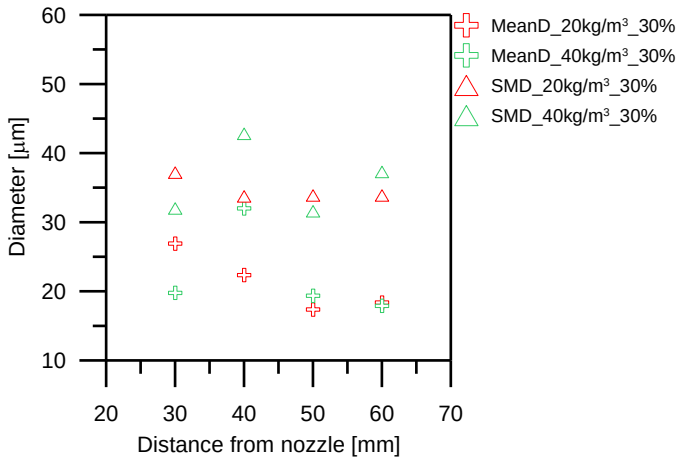

Figure 74. Mean and Sauter mean diameter values at stabilized spray zone for rail pressure of 1500 bar, at different distances from nozzle

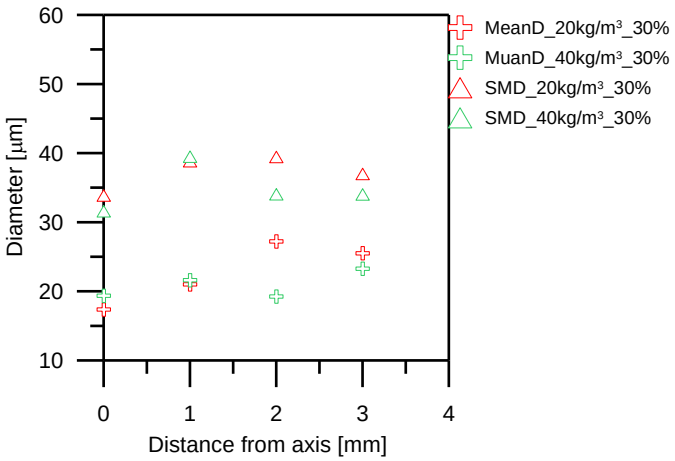

Figure 75. Mean and Sauter mean diameter values at stabilized spray zone for rail pressure of 1500 bar, 50 mm from nozzle at different distances from nozzle

In Figure 72 it can be seen that SMD shows lower values as the injection pressure increases. This behavior is consistent with other results on the bibliography [19]. However, is difficult to state firmly on this theory because in the other three figures is not really clear.

From the side of density, the theory says that droplet diameter should increase with density because a higher coalescence is expected in non evaporative situation. In this case is difficult to obtain a conclusion due to the variability of results, which do not show a remarkable trend in any case.

Figures were represented for only one charge value, because results show that this parameter has no notable influence on droplet diameter. No conclusion can be obtained from the interaction of the charge with rail pressure and ambient density due to the variability of the results.

CONCLUSIONS

The purpose of this task is the study of the influence of the needle lift on the spray droplets velocity and diameter. With this objective, the Continental Direct Acting Injector was successfully installed in the SF6 test rig, which is able to reproduce conventional engine conditions. Moreover, a device to isolate one spray was applied, avoiding disturbances caused by the rest of them.

A methodology was used in order to find the spray axis orientation. Scans at different nozzle distances were carried out to obtain enough points from the axis with which the axis equation (referred to the coordinate bench axis) was obtained.

9 different test conditions were reproduced, combining rail pressure, ambient density and injector charge. Each condition was measured at 10 different positions of the spray: 4 nozzle on-axis distances and 3 off-center locations at two sections. This means a total of 90 test points measured.

Velocity results show that a variation on injector charge has a direct influence on droplet mean velocity. It can be concluded that an increase of needle lift percentage implies higher droplet velocity values. Axial and radial velocity trends are consistent with spray theory.

Apart from this, other conclusions were obtained from the combination of charge variation and other test parameters. On the one hand, it can be observed that a higher charge value is able to overcome the decrease of velocity caused by a higher ambient density, compared with lower value cases. On the other hand, it can be conclude that a raise of charge percentage emphasizes the effect of an increase of rail pressure. As expected, higher injection pressures implies higher droplet velocity values, but in combination with a bigger needle lift this effect is amplified.

Regarding diameter measurements, results are not conclusive. Measurements do not provide enough information to draw any conclusion, due to their low quality and variability.

PDPA technique applied to Diesel sprays presents uncertainty and limitations. Measurements are based on the condition that the laser probe volume is only crossed by just one droplet at a time. This is a constraint very difficult to accomplish for Diesel sprays due to the high droplet density along an injection event. More than one droplet at the volume probe implies a noisy signal generated by the photomultiplier which is really difficult to analyze by the PDPA processor.

Furthermore, all the parameters and settings of the PDPA processor are established by the user criteria. This fact requires some previous knowledge about the technique that the literature cannot offer always due to the especial characteristics of each application.

REFERENCES

1. Hung C. Calvin, Martin J.K, Koo Ja-Ye, "Injection Pressure Effects Upon Droplet Behaviour in Transient Diesel Sprays", SAE Paper 970053

2. Araneo L., Coghe A., Brunello G., Cossali G.E., "Experimental Investigation of Gas Density Effects on Diesel Spray Penetration and Entrainment", SAE Paper 1999-01-0525.

3. Arrègle J., Pastor J.V, Ruiz S., "The Influence of Injection Parameters on Diesel Spray Characteristics", SAE Paper 1999-01-0200

4. Levy N., Amara S., Campoussin J.-C., Guerrassi N., "Non-Reactive Diesel Spray Computations Supported by PDA Measurements", SAE Paper 970049, 1997.

5. Koo J.-Y., Martin J.K., "Droplet Sizes and Velocities in a Transient Diesel Fuel Spray", SAE Paper 900397, 1990.

6. Coghe A., Cossali G.E., "Phase Doppler Characterisation of a Diesel Spray Injected into a High Density Gas under Vaporisation Regimes", Proc. 7th Intl. Symposium of Applied Laser Techniques to Fluid Mechanics, Paper 36.3, Lisbon, 1994.

7. Araneo L., Tropea C., "Improving Phase Doppler Measurements in a Diesel Spray", SAE Paper 2000-01-2047, 2000.

8. Strakey P.A., Talley D.G., Sankar S.V., Bachalo W.D., "The Use of Small Probe Volumes with Phase Doppler Interferometry", Procedeeing 11th ILASS-Americas, Sacramento, CA, pp. 286-290, 1998

9. Koo J.-Y., Martin J.K, "Comparisons of Measured Drop Sizes and Velocities in a Transient Fuel Spray with Stability Criteria and Computed PDF's", SAE Paper 910179, 1991.

10. Allocca L., Belardini P., Bertoli C., Corcione F., De Angelis F., "Experimental and Numerical Analysis of a Diesel Spray", SAE Paper 920576, 1992.

11. Baik S., Blanchard J.P., Corradini M., "Development of Micro-Diesel Injector Nozzles via MEMS Technology and Effects on Spray Characteristics", Atomization and Sprays, vol. 13, pp. 443-474, 2003

12. Smallwood G.J, Gülder Ö.L., "Views on the Structure of Transient Diesel Sprays", Atimisation and Sprays, Vol. 10, pp. 355-386, 2000

13. Su T.F., Chang C.T., Reitz R.D., Farrell P.V, "Effects of Injection Pressure and Nozzle Geometry on Spray SMD and D.I. Emissions", SAE 952360

14. Di Giorgio F., Laforgia D., Damiani V., "Investigation of Drop Size Distribution in the Spray of a Five-Hole V.C.O. Nozzle at High Feeding Pressure", SAE Paper 950087

15. Chehroudi Behrouz, "Preliminary Drop Size and Velocity Measurements in a Dense Diesel-Type Spray", SAE Paper 901673, 1990.

16. Bachalo W.D., "Experimental Methods in Multiphase Flows", Int. J. Multiphase Flow, Vol. 20, Suppl., pp. 261-295, 1994

17. Arcoumanis C., Paa'l G., Whitelaw J.H., "Application of Laser Techniques to Diesel Engine Sprays", Proc. 5th Intl. Symposium of Applied Laser Techniques to Fluid Mechanics, Paper 14.5, Lisbon, 1990.

18. Bachalo W. D., Houser M. J., "Development of the Phase/Doppler Spray Analyser for Liquid Drop Size and Velocity Characterisations", *Proc. AIIA/SAE/ASME 20th Joint Propulsion Conference*, Cincinnati, Ohio, 1984.

19. Soare V., "Phase Doppler Measurements in Diesel Dense Sprays". PhD Thesis. Universidad Politécnica de Valencia, Valencia, España, 2007.

20. Reitz R.D., Bracco F.V., "On the Dependence of Spray Angle and Other Spray Parameters on Nozzle Design and Operating Conditions", SAE Paper 7904

21. Payri R., Araneo L., Shakal J., Soare V., "Phase Doppler measurements: system set-up optimization for characterization of a Diesel nozzle", *Journal of Mechanical Science and Technology 22 (2008), 1620 ~1632.*

3.1.2 Modelling of Emission Formation and Exhaust Gas Aftertreatment – Summary of Experimental Work At CMT Test Facility

UNIVERSITAT POLITÈCNICA DE VALÈNCIA

motores térmicos

Modelling of Emission Formation and Exhaust Gas Aftertreatment

Summary of experimental work at CMT test facility

Graz, May 8th 2012

JV Pastor
JM Garcia-Oliver
JM Pastor
C Mico
W Vera-Tudela
V Calabuig

CONTENTS

- Reacting spray
  - Experimental methodology
  - Test matrix
  - Sample of results

REACTING SPRAY

Objective

- Experimental characterization of diesel flame for fuels already studied under inert conditions

Heat Release	• Pressure signal • Luminosity delay: Photodiode
Flame Lift-off	• OH* visualization
Soot	• Laser Extinction Method (LEM) • Laser Induced Incandescence (LII) • Two-Colour Pyrometry (2C)
Temperature	• Two-Colour Pyrometry (2C)

3

REACTING SPRAY

Optical Arrangement

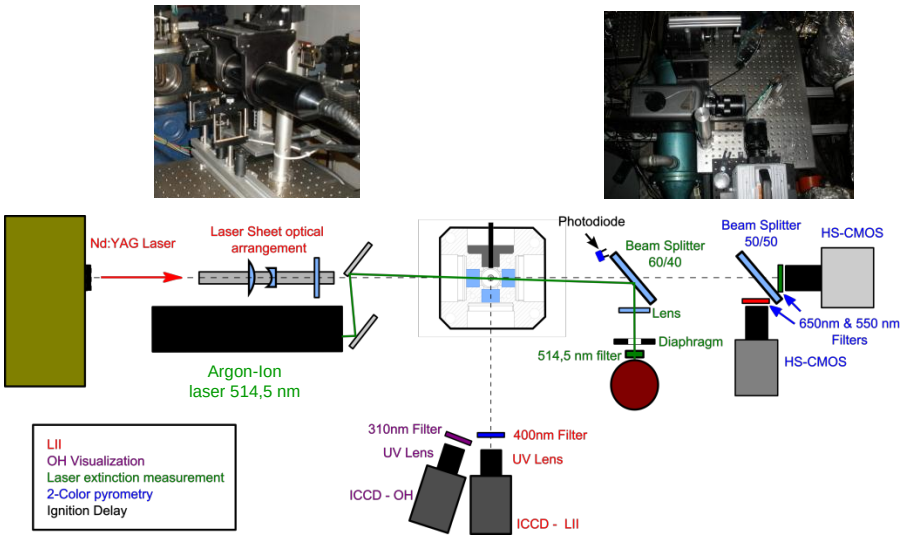

4

REACTING SPRAY

Optical Arrangement

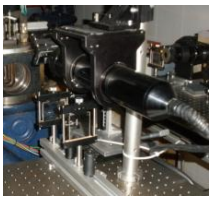

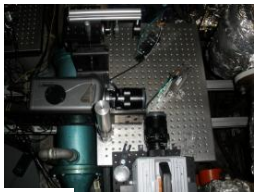

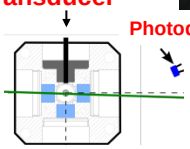

LII
OH Visualization
Laser extinction measurement
2-Color pyrometry
Ignition Delay

UNIVERSITAT POLITÈCNICA DE VALÈNCIA
motores térmicos

REACTING SPRAY

Optical Arrangement OH* Visualization

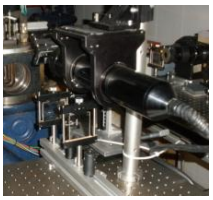

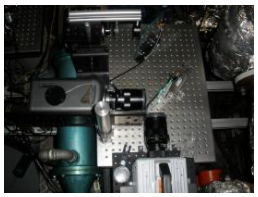

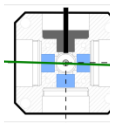

LII
OH Visualization
Laser extinction measurement
2-Color pyrometry
Ignition Delay

REACTING SPRAY

OH* Visualization

- OH* radiation at 310nm is recorded by an intensified camera
  - Andor IStart ICCD
  - UV Lens - FL=105 mm , f#=4
  - Gate = 800 µs @ 2200 us after SOE (800us prior to LII)
- Distance between first OH* detected downstream and nozzle tip is Lift-Off Length (LOL)
- Processing routine:
  - Image thresholding
  - Definition of the flame axis
  - Calculation of the minimum distance to the nozzle

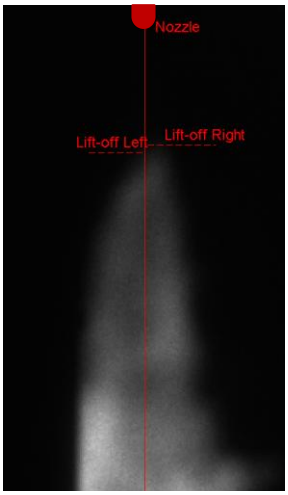

UNIVERSITAT POLITÈCNICA DE VALÈNCIA
REACTING SPRAY
motores térmicos

OH* Visualization

- Example of LOL scattering
  - D0-53bar-900K-1000bar

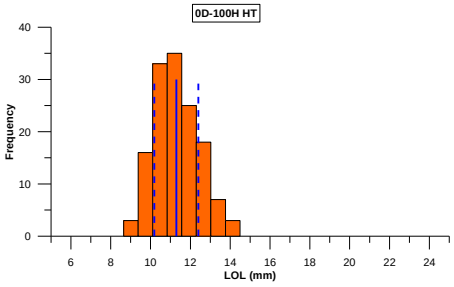

- Example of results for Prail variation (HT)

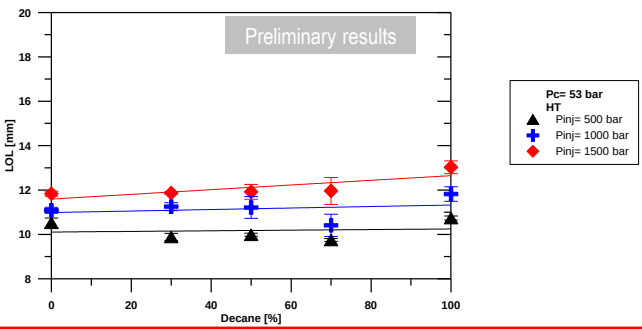

REACTING SPRAY

Optical Arrangement — Laser-Extinction (LEM)

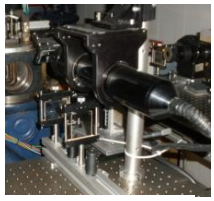

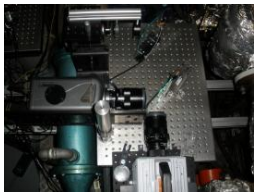

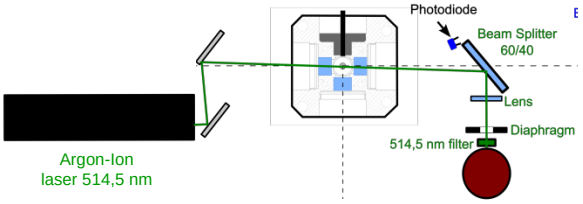

LII
OH Visualization
Laser extinction measurement
2-Color pyrometry
Ignition Delay

UNIVERSITAT POLITÈCNICA DE VALÈNCIA
REACTING SPRAY
motores térmicos

Laser Extinction

- A CW laser beam @ 514.5 nm crosses the flame with an intensity (I_0), which is attenuated (I) due to the presence of soot
  - Laser Waist ~0.1 mm
- Based on Beer-Lambert Law, soot characteristic KL_{LEM} is obtained with temporal resolution:

$$KL_{LEM} = -LN\left(\frac{I}{I_0}\right)$$

- Point measurement → Limited spatial resolution
  - Measurements at 5 positions in the combustion chamber

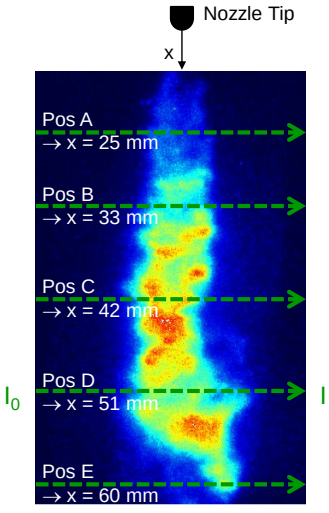

Laser Extinction

- Example of cycle-to-cycle scattering

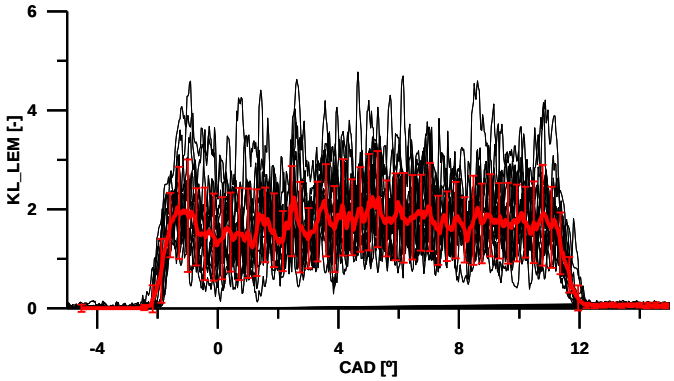

Optical Arrangement LII

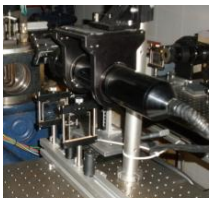

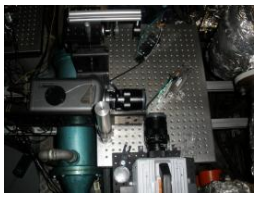

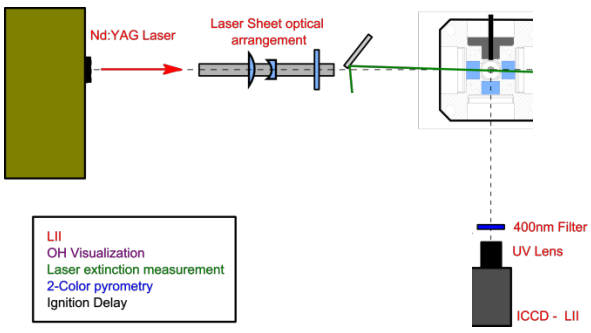

REACTING SPRAY

Laser Induced Incandescence (LII)

- A pulsed Laser sheet (Nd:YAG) crosses the flame l = 1064 nm to avoid PAH fluorescence
  - t_{laser} = 10 ns @ 3001 us ASOE
  - Energy » 450 mJ/pulse
  - Sheet Height x Width = 45 x 0.35 mm^2
- Soot particulates are heated to very high temperature, images are recorded
  - Dynamight ICCD
  - UV Lens – FL=100 mm, f#=2
  - Gate = 50 ns @ 3001 us ASOE

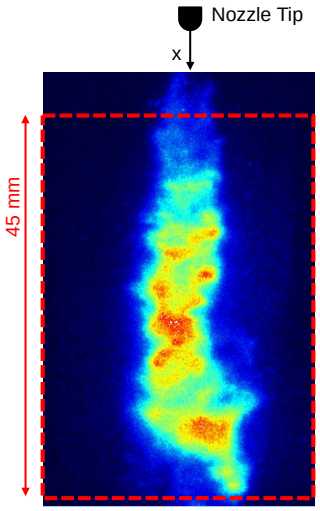

14

REACTING SPRAY

Laser Induced Incandescence (LII)

- Soot induced incandescence can be separated from off-sheet natural flame luminosity due to its higher intensity
  - A LP filter @400nm improves the separation between both sources of incandescence radiation
- LII signal is proportional to soot volume fraction
- KL from LEM can be used as a comparison of LII images
  - Integration of LII along a LEM path

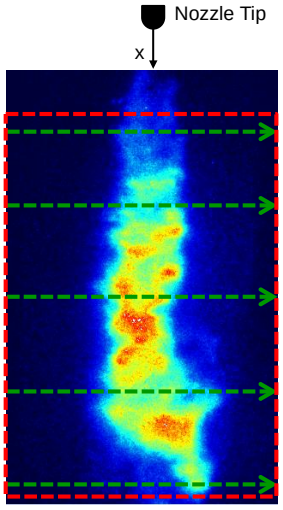

15

REACTING SPRAY

Laser Induced Incandescence (LII)

- Processing routines
  - Background luminosity substraction + Thresholding

16

REACTING SPRAY

Laser Induced Incandescence (LII)

- Processing routines
  - Example of LII scattering

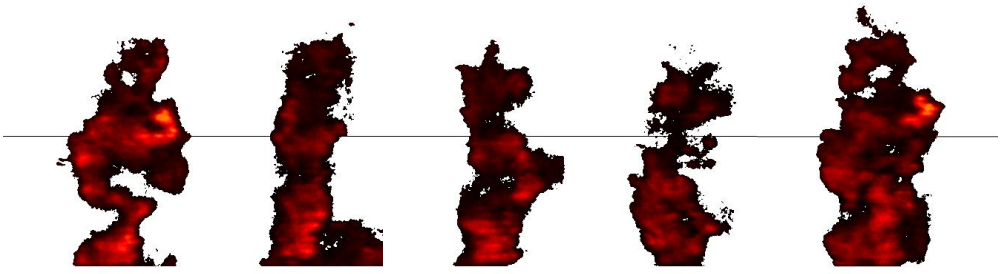

17

REACTING SPRAY

Laser Induced Incandescence (LII)

- Processing routines
  - Statistics from images

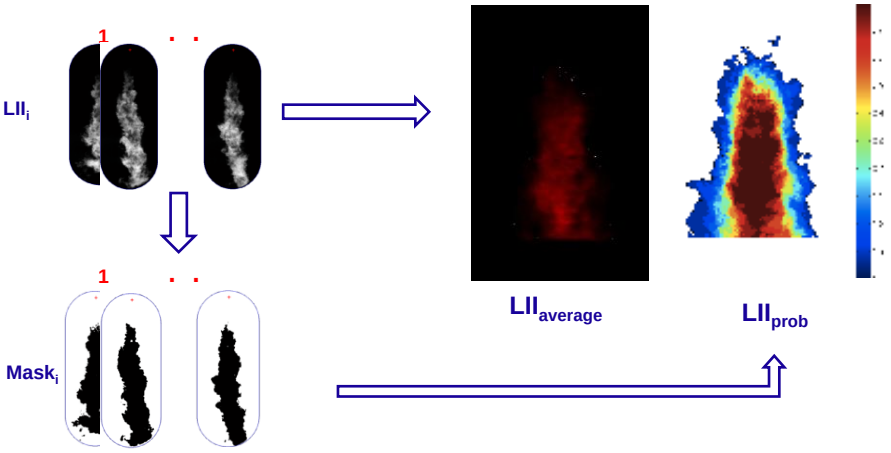

UNIVERSITAT POLITÈCNICA DE VALÈNCIA
REACTING SPRAY
motores térmicos

Laser Induced Incandescence (LII)

- Processing routines
  - Calculation of spatially resolved parameters
    - Geometry: Flame Width L(x)
    - Radially integrated cummulative intensity

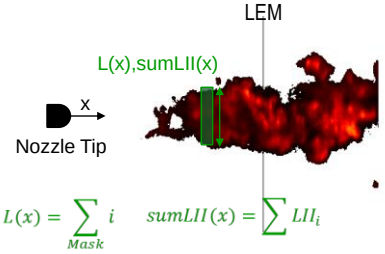

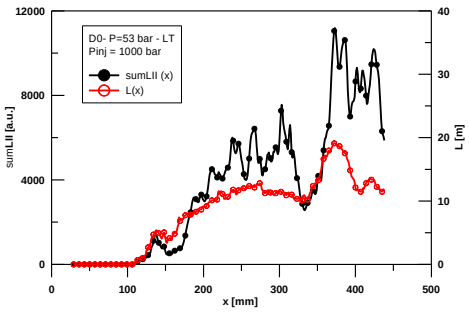

REACTING SPRAY

Laser Induced Incandescence (LII)

- Example of scattering

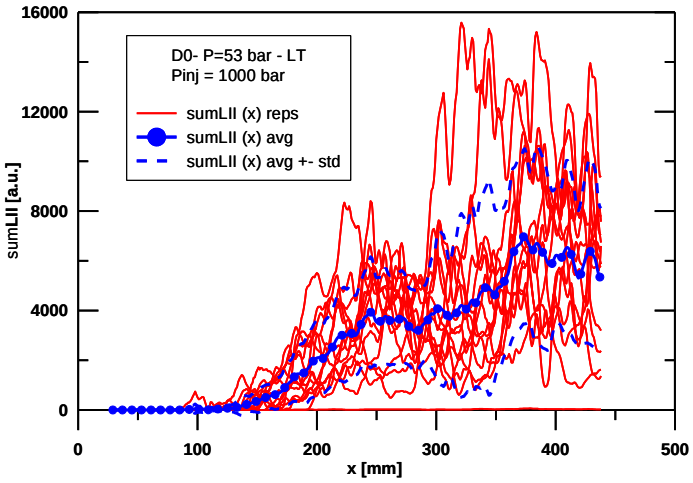

20

REACTING SPRAY

Laser Induced Incandescence (LII)

- Processing routines
  - Calculation of area-integrated parameters
    - Geometry: Area
    - Cummulative intensity

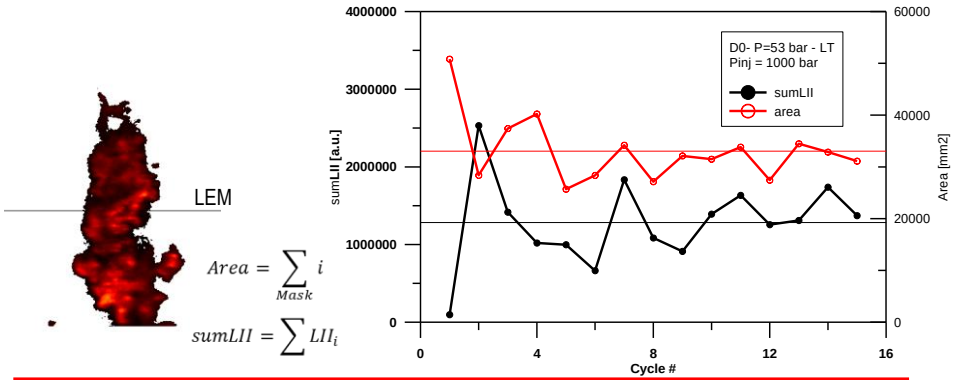

21

REACTING SPRAY

Optical Arrangement — 2C Pyrometry (2C)

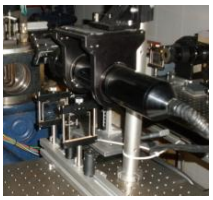

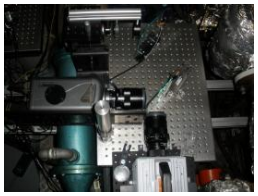

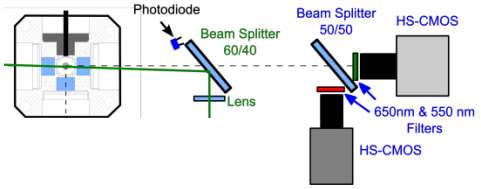

LII
OH Visualization
Laser extinction measurement
2-Color pyrometry
Ignition Delay

REACTING SPRAY

2-Color Pyrometry (2C)

- Natural flame luminosity at 650 and 550nm is registered simultaneously by two High-Speed CMOS cameras.

$$I_{soot}(\lambda, KL_{2C}, T) = \left(1 - exp\left[-\frac{KL_{2C}}{\lambda^{\alpha}}\right]\right)\frac{C_1}{\lambda^5}\frac{1}{exp\left[\frac{C_2}{\lambda T}\right] - 1}$$

- Both intensities at each pixel are combined to obtain KL and Temperature distributions

650nm 550nm

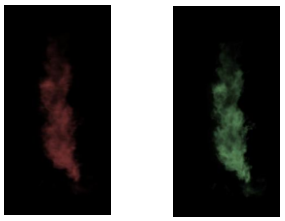

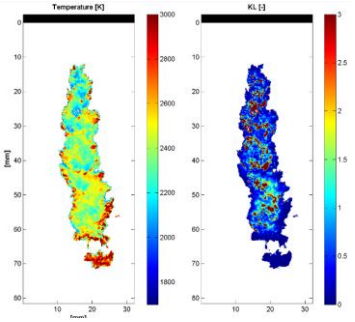

REACTING SPRAY

2-Color Pyrometry (2C)

- l = 650 nm
  - Digital High-speed Camera Phantom V12.1
  - Resolution: 384x960 @ 15000 fps (Dt=66.6us ≈ 0.2 CAD)
  - Exposure time: 5-8 μs
  - Lens: Zeiss FL100mm f/# 2.0

- l = 550 nm
  - Digital High-speed Camera Photron SA5
  - Resolution: 384x960 @ 15000 fps (Dt=66.6us ≈ 0.2 CAD)
  - Exposure time: 6.6-11μs
  - Lens: Zeiss FL100mm f/# 2.0

UNIVERSITAT POLITÈCNICA DE VALÈNCIA
REACTING SPRAY
motores térmicos

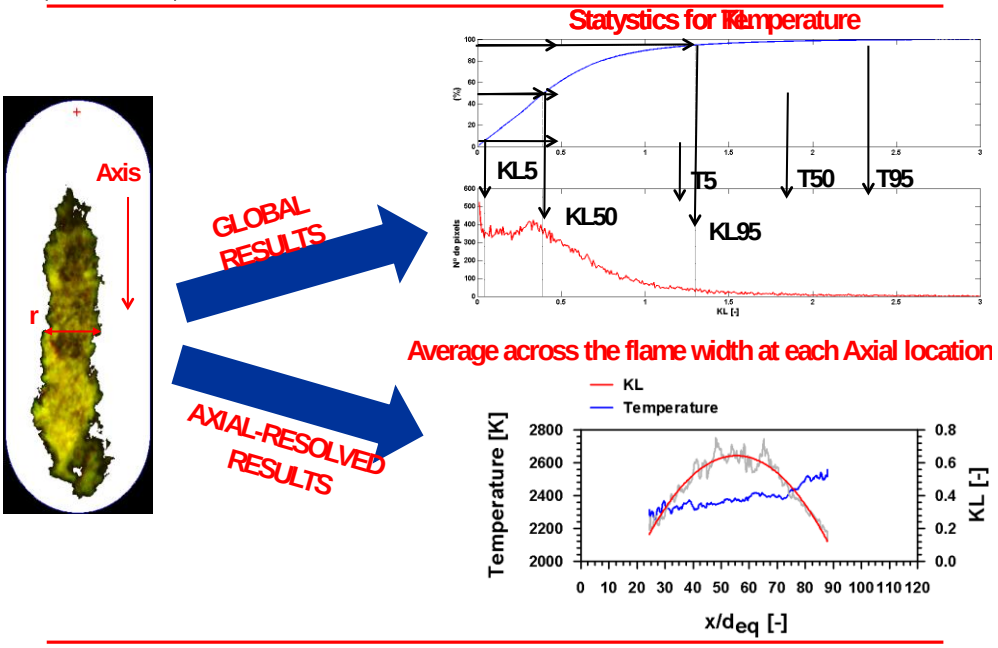

REACTING SPRAY

Test matrix

- Parametric studies

Parameter	Fuel	PTDC [bar]	TTDC [K]	Prail [bar]	Tests	LEM pos
Baseline	D100\D70\ D50\D30\D0	53	800\900	1000	10	ABCDE
Prail	D100\D70\ D50\D30\D0	53	800\900	500/1000/1500	20	BD
P	D100\D70\ D50\D30\D0	43\53\73	800\900	1000	20	BD

26

REACTING SPRAY

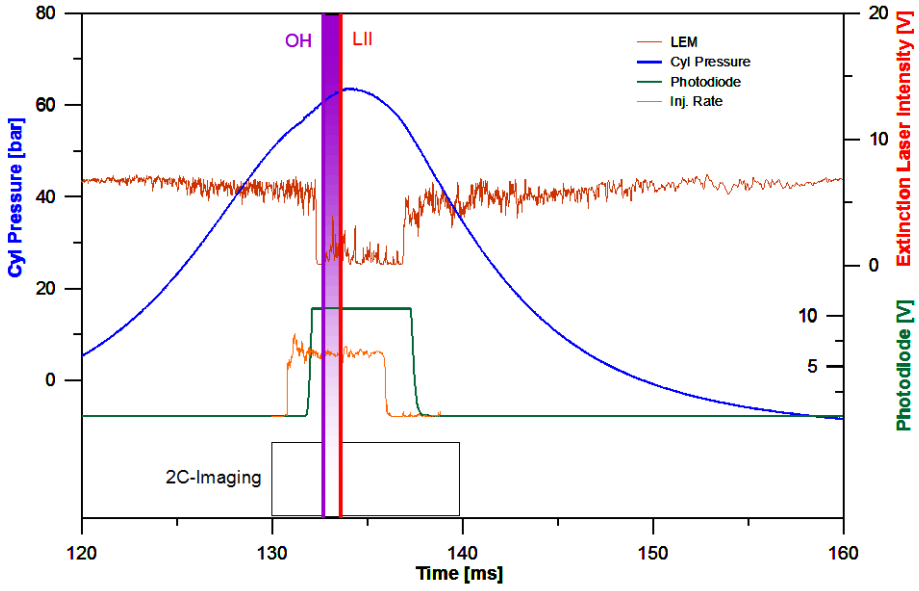

27

REACTING SPRAY

Test matrix

Parameter	Fuel	PTDC [bar]	TTDC [K]	Prail [bar]	P/PD/LE [cycles]	OH*/LII [images]	2C [image$_2$]
Baseline	**D100\D70\ D50\D30\D0**	53	**800\900**	1000	1000	1000/750	75000
Prail	**D100\D70\ D50\D30\D0**	53	**800\900**	**500/1000/1500**	800	400/300	30000
P	**D100\D70\ D50\D30\D0**	**43\53\73**	**800\900**	1000	800	400/300	30000
				TOTAL:	2600	1800/1350	135000

REACTING SPRAY

Summary of status

- Facility & optical setup preparation: December-January
- Test campaign: February-April
  - Simultaneous recording of Set#2&3 LL
  - Experimental problems with Hexadecane
- Processing & analysis
  - Processing has been done for all techniques, except for the 2C routines

D0 – 53 bar – 1000 bar - LowT

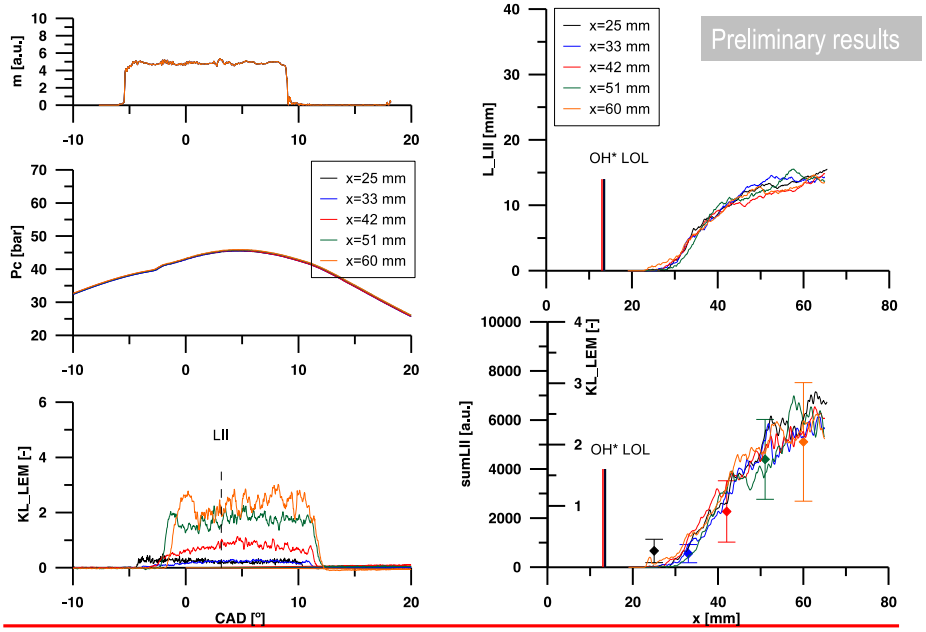

31

D0 – 53 bar – LowT

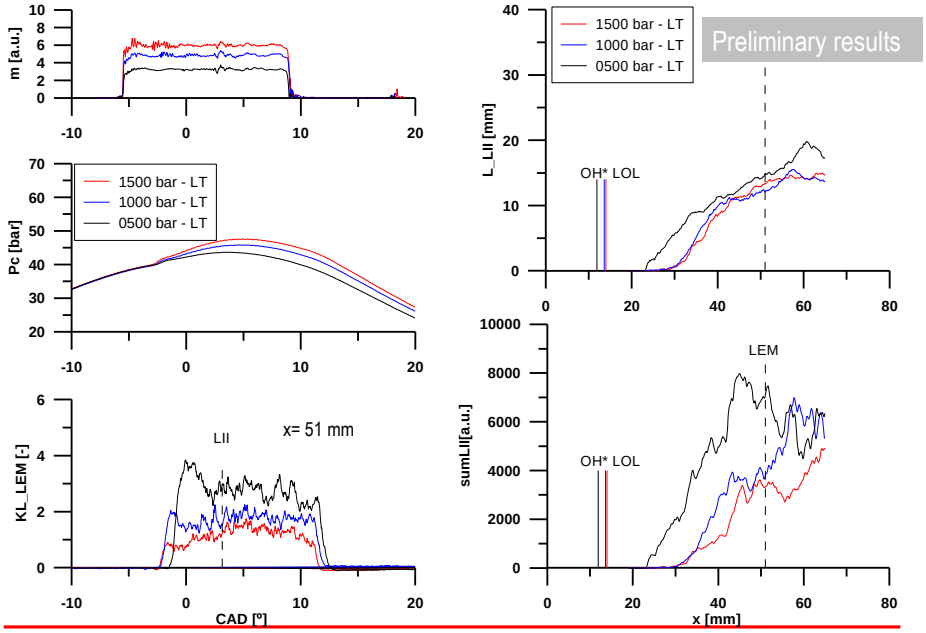

33

D0 – 1000 bar – LowT

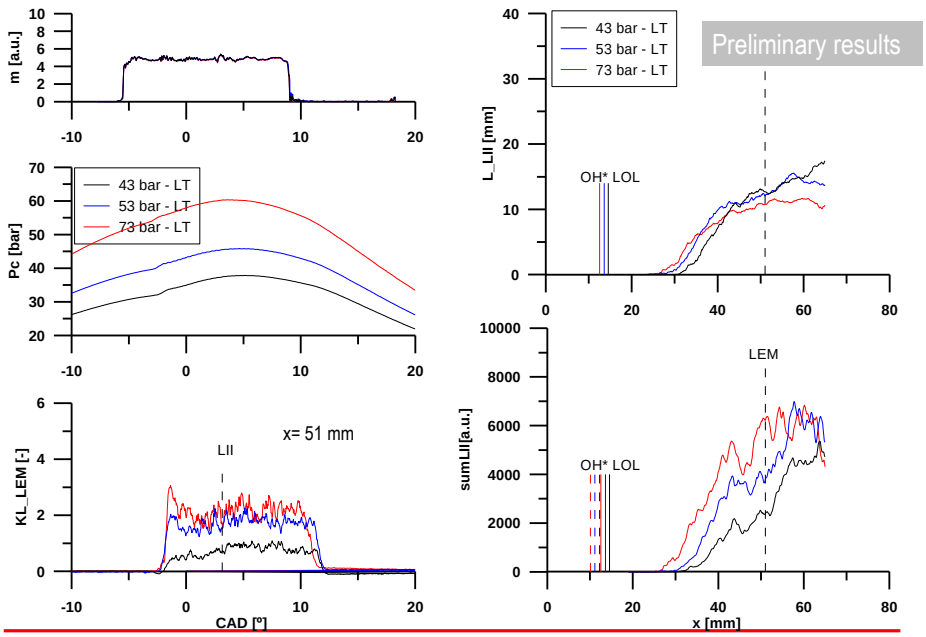

REACTING SPRAY

Deliverables

- To be defined according to CFD validation
- Different techniques can produce comparable parameters

Parameter	PRESSURE	PHOTODIODE	OH* IMAGING	LEM	LII	2C
t DELAY	X	X				X
LOL			X			X
SREACT						X
Area/L					X	X
KL/SOOT				X	X	X
T						X

3.2 Publicaciones

3.2.1 A Spectroscopy Study of Gasoline Partially Premixed Compression Ignition Spark Assisted Combustion

A Spectroscopy Study of Gasoline Partially Premixed Compression Ignition Spark Assisted Combustion

J.V. Pastor[1], J. M. García-Oliver[1], A. García[1*] and C. Micó[1] and R. Durrett[2]

[1]CMT- Motores Térmicos - Universidad Politécnica de Valencia, Camino de Vera s/n 46022 Valencia - SPAIN

[2]Diesel Engine Systems Group - Propulsion Systems Research Lab GM R&D Center, MC: 480-106-252, 30500 Mound Rd, Warren, MI 48090-905

(*) CORRESPONDING AUTHOR:

Dr. Antonio Garcia: angarma8@mot.upv.es

Telephone: +34 963879659

Fax: +34 963877659

ABSTRACT

Nowadays many research efforts are focused on the study and development of new combustion modes, mainly based on the use of locally lean air-fuel mixtures. This characteristic, combined with exhaust gas recirculation, provides low combustion temperatures that reduces pollutant formation and increases efficiency. However these combustion concepts have some drawbacks, related to combustion phasing control, which must be overcome. The aim of the present work is to study the integration of combustion phasing control by means of a spark plug ignition system in a CI engine working in a partially premixed combustion (PPC) mode when very low fuel reactivity is used.
Tests have been performed in an optical engine by means of broadband radiation imaging and emission spectrometry. The engine hardware is typical of a compression ignition passenger car application. Gasoline was used as the fuel due to its low reactivity. Combining broadband luminosity images with pressure- derived heat- release rate and UV- Visible Spectra, it was possible to identify different stages of the combustion reaction. After the spark discharge, a first flame kernel appears and starts growing as a premixed flame front, characterized by a low and constant heat-release rate. The heat released increases temperature and pressure inside the combustion chamber, which causes the auto-ignition of the rest of the unburned mixture. The rate of heat release at this point is more pronounced, due to an auto-ignition phenomena and the propagation of the reactions through the combustion chamber is faster than in the other stages. The measured UV-Visible spectra showed the presence of radicals marking different combustion phases.

KEYWORDS:

PPC, Spark assistance, Gasoline fuel, Optical Investigation, Combustion description

HIGHLIGHTS

- Spectra of a novel combustion mode is described with spatial and time resolution
- PPC combustion combined with spark assistance and gasoline fuel on a CI engine
- UV-Visible spectrometry, high speed imaging and pressure diagnostic, employed on the analysis.
- Chemiluminescence of different chemical species describes the progress of combustion reaction.

NOMENCLATURE

CI	Compression Ignition
ICE	Internal combustion engine
EGR	Exhaust gas recirculation
PPC	Partially premixed combustion
SACI	Spark assisted compression ignition
ROHR	Rate of heat release
CAD	Crankangle degree
ACV	Apparent combustion velocity

1. INTRODUCTION

Nowadays the automotive scientific community focuses part of their efforts on the investigation of new combustion modes [1] with the aim of reducing fuel consumption and emissions in CI (Compression Ignition) diesel engines [2, 3]. These modes are mainly characterized by taking place under lean locally homogeneous air-fuel mixture conditions which, combined with high exhaust gas recirculation rates, provide low combustion temperatures. As a consequence, NOx and soot formation are reduced while fuel consumption and efficiency improve [4].

In spite of their benefits, these combustion concepts present some challenges that must be overcome before their practical implementation in ICEs. The main limitation is obtaining a proper combustion phasing and control over a wide range of engine load and speed. Highly-premixed combustion modes in CI engines are dominated by chemical kinetics, which are directly dependent on temperature and chemical composition of the mixture. As a consequence, achieving the proper ignition conditions requires both adequate mixing and temperature of the charge. To solve this problem, different strategies have been proposed [5-7]. Temperature can be controlled by intake air heating or modifying the compression ratio. Other strategies like control of EGR rate or the amount of trapped combustion gases also modifies mixture composition. Multiple injection strategies and combinations of different fuels have also been investigated. However, the majority of the techniques mentioned cannot provide precise control over the combustion phasing, since they require time scales too large to achieve cycle-by-cycle control.

All previous actions try to compensate the high chemical reactivity of the diesel fuel that does not provide enough mixing time before the start of combustion. Thus, recent studies have tried to overcome these disadvantages by using fuels with different reactivities. PPC (Partially Premixed Combustion) is a novel combustion strategy with the main characteristic being the use of a low reactivity fuel [7, 8, 9]. This combustion mode is in transition between normal diffusion combustion in CI engines and Premixed Charge Compression Ignition (PCCI). It allows a high degree of fuel-air mixing before ignition but the charge is not completely homogeneous [11, 12]. Nevertheless, while all these solutions provide some control of the combustion phasing, they still cannot deliver the required cycle-to-cycle control capability of these partial or fully premixed combustion processes. Moreover, when a very low reactivity fuel is used [13], it is not possible to achieve stable engine operation for light and mid load conditions.

Spark assisted combustion phasing and control has been investigated for controlled auto-ignition (CAI) implementation on port fuel injection SI engines. The spark plug has been used to supply the necessary energy for achieving a controlled auto-ignition process with a method referred to as Spark Assisted Compression Ignition (SACI). In this mode, the combustion process is composed of a first growth of a reaction kernel, due to the energy supplied by the spark, which leads to the start of a propagating flame. The flame propagation combustion consumes part of the fuel, releasing energy that increases the mixture temperature and provokes its auto-ignition. Since flame propagation is generally slower than auto-ignition, this mechanism reduces the overall heat release rate. Previous experimental work using spark ignition engine architecture [14, 15] and moderate reactivity fuels suggests that this method can provide good combustion phasing while the response time is short enough for cycle-by-cycle application [16, 17].

The aim of the present work is to study the integration of combustion phasing control by means of a spark plug ignition system in a CI engine working in partially a premixed combustion (PPC) mode, when very low fuel reactivity is used. On one hand, the spark plug offers a cycle-to-cycle control over PPC regardless of thermodynamic conditions. On the other hand, the use of a CI engine which is not common in the SACI literature, was chosen in order to overcome some previously reported problems related to the use of high octane fuels like misfiring under light load engine conditions. Experiments have been performed in an optical engine, with a diesel-like compression ratio and geometry and equipped with a common rail injection system enabling high-pressure injection, EGR and temperature control. Moreover, the experimental work was carried out using gasoline, because of its low reactivity. Since the investigation was performed in an optical engine, different tools were combined in the study: in-cylinder pressure analysis, combustion broadband imaging and emission spectrometry.. Emission spectrometry has been proven as a powerful tool for analysis of new combustion modes, so it is used to develop a detailed description and improve the existing knowledge about the phenomenology of the gasoline partially premixed combustion compression ignition mode with spark assistance. Therefore, the main objective of the work is the improvement of the fundamental understanding of this combustion process.

2. EXPERIMENTAL TOOLS AND MEASUREMENT PROCEDURE

2.1. Engine

The experimental work was performed at a low load-operation mode on a 4-stroke DI diesel single cylinder optical engine (Fig.1) with the specifications listed in Table 1. It is equipped with an elongated piston and a cylindrical bowl, with dimensions of 45 x 18 mm (diameter x depth), allowing optical access to the combustion chamber through a sapphire window located at its bottom. Below the piston bowl an elliptical UV mirror is placed at 45º, aligned with the piston axis.

The cylinder head is a modified 2.2 HSDI 4 valve diesel cylinder head. One of the exhaust valves was removed in order to install a spark plug. This modification does not strongly affect air management, due to the low operating engine speed and the skip fire methodology used in this work. The engine is equipped with a conventional common rail injection system. The injector is positioned at the center of the combustion chamber and oriented so that one of the jets passes through the spark electrodes. Tests were conducted in skip-fire mode to prevent fouling of the optical access and minimize thermal engine gradients; thus, only one injection is performed every 30 cycles. This methodology ensures repetitive engine conditions between fired cycles.

In-cylinder pressure is measured, and thermodynamic analysis is performed with a one-zone model CALMEC [19, 22]. This diagnosis tool uses the measured in-cylinder pressure as the main input and other engine parameters as boundary conditions of the test. The model's main result is the Rate of Heat Release (ROHR). Time resolution for these variables depends on the crank angle encoder configuration (0.2 CAD).

All the tests were carried out under the same engine conditions. Engine speed was set to 750 rpm. This low regime offers a long cycle and combustion duration, which are optimum conditions to check the viability of the combustion mode. Intake air temperature and pressure were set to 303 K and 1.6 bar respectively. O2 concentration inside combustion chamber is controlled using a synthetic EGR

system, where EGR gases are substituted only by N2. For this study, XO2 was fixed at 18%. Fuel was commercial gasoline with 95 octane number and 765 kg/m3 density. The start of injection was located 19 crank angle degrees before top dead center, injecting 20.6 mg of fuel per cycle, which results in an average 0.35 equivalence ratio. Due to the low reactivity of the fuel, no ignition occurs under these operating conditions when no spark plug discharge is performed. The spark discharge was located at -10 CAD, coinciding with the end of injection, while the local air-fuel mixture around the spark plug is still rich enough and thermodynamic conditions are adequate for ignition. To enable an adequate mixture preparation in the spark plug zone within the required time scales, injection pressure was set to 600 bar. This pressure is higher than the usual range offered by commercial direct injection gasoline systems, so a common rail Bosch-Piezo system was used.

2.2. Optical Apparatus

Digital imaging and spectroscopic analysis in the UV-Visible range were performed. Light emitted by the combustion process is reflected by the UV Mirror and guided to both a high speed camera and a spectrograph. The optical set-up is shown in Fig. 2.

In order to register temporal and spatial evolution of broadband radiation from the combustion process a Photron Fastcam Ultima APX camera was employed. This High Speed CMOS camera was used to record at 6000 fps with a 512 x 512 pixels resolution. The exposure time was fixed at 166.7 µs (approx. 0.75 CAD), ensuring a good dynamic range although soot emission could saturate the images. The lens used is a Zeiss 100mm f/2 ZF Makro-Planar, keeping the aperture constant for all the tests. This element restricts the bandwidth of light recorded to the visible range. The whole optical system provides an effective resolution of 0.17mm/pixel for the images.

A Jovin Yvon Horiba Triax 180 spectrograph was used to decompose the light emitted by combustion in the UV-Visible range, which was coupled with a LaVisionDynamight intensified CCD camera. A grating with 300 groove/mm was used which, combined with the 512 x 512 pixels of the ICCD camera, allows detecting a wavelength bandwidth of 170 nm. Two different configurations were chosen, the first one with the grating centered at 350 nm (265-435 nm) for the UV range and the other one centered at 450 nm (365 – 535 nm) for the visible range. The entrance slit width was set to 0.3 mm and the exposure time of the ICCD camera was 500 µs (approx. 2.25 CAD). A UV-Lens (Ø25.4 - 100 mm focal length) was used to focus the light inside the spectrograph.

2.3. Image Processing

A processing routine was applied to the high speed camera images, to obtain numerical information about the size and shape of the combustion area for further analysis. Each image was binarized considering a fixed threshold value, so pixels corresponding to the flame (higher intensity than threshold) are assigned a value of 1, while pixels of the background (lower intensity than threshold) are assigned a value of 0. Flame area is defined as the addition of all pixels set to 1. In a second step, the contour of the flame was obtained from the binarized image. Fig. 3 presents an example of the different processing steps.

For the analysis of the flame propagation velocity, a geometrical magnitude was defined. Fig. 4 shows that flame shape changes during the combustion cycle. The first steps of the reaction are characterized by a geometrically continuous flame, there is a middle stage when the flame shrinks and breaks into different parts. In order to characterize this behavior, the time derivative of the ratio between flame area and contour length is obtained. In this way, not only a change of flame area is characterized but also its fragmentation due to a reaction slowdown. From now on, this magnitude will be named as apparent combustion velocity (ACV).

3. RESULTS AND DISCUSSION

3.1. Analysis of flame radiation images

A first description of the phenomena involved in partially premixed compression ignition spark assisted combustion can be obtained from the analysis of the natural luminosity released by reaction. Fig. 4 shows a crankangle resolved sequence of images of a combustion cycle. For brevity, only one out of two recorded images are shown. After the spark discharge (-10.0 CAD), a high luminosity area is observed around the spark plug (-10.3 CAD). This active site shifts towards the combustion chamber wall, and later on slightly reduces in size but it does not change in position. At -7.4 CAD, however, the luminous area is seen to have expanded, but its appearance is different: the original high intensity spot from the spark discharge still exists, but it is surrounded by a much larger compact zone with dimmer intensity. This zone seems to be expanding to the rest of the combustion chamber but, after -4.6 CAD, it reduces in size again, becoming less compact in appearance. This reduction phase finishes at -0.3 CAD, from which a second increase in luminous area is observed. During this phase, the luminous area progresses towards the rest of the combustion chamber, with a relatively low intensity appearance except for some locally bright spots that will be discussed below. After 7.0 CAD, the radiation zone starts to reduce again, but this time it leads to the extinction of the reaction zone.

The previous qualitative sequence can be analysed in terms of quantitative variables derived from in-cylinder pressure and image processing as shown in Fig. 5. The evolution of the combustion area is in agreement with the previous images: spark discharge occurs at -10.0 CAD, and no large increase in area occurs until approximately -8.0 CAD, as shown in the ACV evolution. During that interval, only the spark generated radiation occurs. From -8.0 CAD to approximately -2.0 CAD (minimum value in area after the first maximum) the phase of the compact radiation area evolution occurs. From -2.0 CAD onwards, a second combustion period occurs with the corresponding increase in area. Both phases are marked by a corresponding ACV peak. It is noticeable that all three periods can also be observed to be approximately coincident with those observed in the pressure-derived heat release rate, namely a first phase without heat release from spark timing to -9.0 CAD, a second period with a sustained heat release until -1.0 CAD, after which a third period with a noticeable peak in heat release occurs. Both differences between second and third phases in heat release values and, to a lower extent, in area and ACV, indicate that the last one is faster than the second one.

Previous analysis of quantitative parameters makes it possible to define three different stages during the combustion process. After the spark discharge, a growth of an early flame kernel takes place with negligible heat release. The kernel phase it is followed by a flame front propagation under premixed conditions. Energy released by premixed reaction causes an increase in temperature and pressure in the combustion chamber, leading to the autoignition of the rest of the mixture. The mean

difference between autoignition and premixed combustion phases is the propagation rate and, as a consequence, the maximum values attained by the rate of heat release. Moreover, it can be seen that reaction is not uniform along the combustion chamber. While the premixed combustion takes place around the spark plug, the auto-ignition phenomenon extends to the whole field of view. The description obtained is consistent with the work of other authors, such as Natarajan and Tornatore [17, 23].

3.2. Analysis of radiation spectra

Spectral analysis is useful in order to better investigate the combustion process. In the literature, different chemical species and radicals are identified as good tracers of the stages of a hydrocarbon combustion reaction. Thus their presence changes radiation emission spectra and helps describe the evolution of the reaction.

Due to optical apparatus limitations, spectra were registered at different locations along the combustion chamber in order to obtain good spatial resolution. For the analysis, the combustion chamber was divided into nine regions of interest (Fig. 6). The size of each region is 79 x 16 pixels and had an area of 13.5 x 2.7 mm. Each region is labeled according to the horizontal (1,2,3) and vertical (T,C,B) location.

The different spectra registered during the combustion process are presented in Fig. 7 to Fig. 10. All of them correspond to central location in the chamber (1C, 2C and 3C). Results in other locations are similar. Each figure shows instantaneous spectra from two different engine cycles, as two recordings were done for each of the visible and UV wavelength ranges, however both overlap in the 400-440 nm interval. Representative timings are shown for the following combustion phenomena: 1. Spark discharge and flame kernel appearance (Fig. 7); 2. Flame growth under premixed conditions (Fig. 8); 3. Auto-ignition combustion (Fig. 9). Fig. 10 corresponds to the late combustion phase.

Fig. 7 shows spectra recorded between -10.8 and -8.5 CAD, which corresponds approximately to the interval between spark discharge and start of heat release. Light is mainly produced by the plasma generated around the spark plug terminals (zone 1C). The early interactions between excited hydrocarbon species and the air are represented by the presence of CN and NH peaks, according to the literature [23]. Moreover, the corresponding spectrum also shows two weak peaks from OH and CH emission (310 and 430 nm). Both radicals are indicators of combustion chemical reactions associated with the formation of an early flame kernel. Due to the low reaction rate during the first stage of combustion, no evidence of radical or chemical activity was detected in the rest of the combustion chamber, so no information is shown for zones 2C and 3C.

Spectra between -5.5 and -3.2 CAD correspond to the second phase of the heat release rate, where the premixed combustion reaction is progressing. These are shown in Fig. 8. The spectrum around the spark plug (1C) is similar to blackbody continuum emission. A noticeable peak of OH (310 nm) is also present. Both characteristics are a consequence of combustion occurring in fuel rich zones, with soot particles forming as a result of the accumulation of fuel close to the combustion chamber wall. At position 2C (injector), the spectra are composed only of chemiluminiscence radiation. Apart from the intense OH and CH peaks (310 and 430 nm), there is also a continuum band, starting at 270 nm and extending into the visible range. This band is usually attributed to HCO (Vayda bands, from 270 to

410 nm [24]) and HCHO radiation (Emelus bands, from 340 to 523 nm [24]). Both radicals are representative of the transition from low to high temperature combustion. According to the radiation images (Fig. 4) the reaction has reached position 2C, and therefore the recorded spectra correspond to a premixed front progressing towards the unburned mixtures. At position 3C, it was not possible to identify either radicals or chemical reactions due to the low emission levels, so spectra are not shown.

Fig. 9 shows spectra recorded during the 2 to 4.3 CAD interval, when the main auto-ignition process is underway. At location 1C the OH peak is still present, but the continuum spectrum of soot is more doubtful. Instead, spectra suggest the presence of CO as a broadband radiation between 420 and 490 nm. Both facts are consistent with the final stages of a combustion process, when soot radiation has almost disappeared, and radiation of late occurring species like CO appears [23, 24]. On the other hand, at position 2C the auto-ignited combustion is taking place. Here the recorded spectra are governed by broadband continuum emission and an intense peak of OH (310 nm). Radiation images (Fig. 4) also indicate very strong luminosity in the injector area. Both diagnostics hint at the presence of soot particulates (bright spots). This interpretation is consistent with fuel leakages observed from the injector, which ignite as a consequence of local high temperatures and, due to the lower mixing rate, form a diffusion flame. Finally, at position 3C CH and OH peaks (430 and 310 nm) can be identified, and HCO and HCHO background emission is also present. Both indicate a relatively similar emission as in location 2C, from -5.5 to -3.2 CAD, except for the stronger CH and weaker OH in this case compared to -5.5 to -3.2 CAD spectra. Such differences can be explained by the different combustion regime (premixed at 2C from -5.5 to -3.2 CAD vs auto-ignition at 3C from 2 to 4.3 CAD).

Finally, Fig. 10 shows the spectra during the interval from 5.8 to 8.0 CAD when the combustion process is nearing completion. The spectrum measured at position 3C shows a weak OH peak at 310 nm and a broadband component, which extends to the visible range, characteristic of CO-O produced from the oxidation of HCO and HCOH. This emission overlaps possible peaks of other radical like CH at 430 nm. This spectrum is common in the major part of the combustion chamber at this stage except around the injector (2C), where the influence of fuel leakages is still present and spectra show a more intense OH peak and soot broad-band emission.

4. CONCLUSIONS

Direct visualization and spectroscopic analysis of natural radiation has been combined with the analysis of the Rate of Heat Release to provide a description of the combustion process occurring in a Partially Premixed Spark Assisted Compression Ignition mode using gasoline. Three different stages of combustion have been identified. The process starts with the spark discharge, which produces a flame kernel around the spark plug that later evolves to a premixed flame front. This premixed flame front heats unburned mixture and progresses into an auto-ignition combustion that burns out the rest of the charge.

Spectra of the combustion process change as the process evolves. During the first step of the reaction (-10.8 CAD), the main radiation comes from the spark discharge and the early flame kernel formed around the spark plug. The spectra is characterized by the emission due to early interaction between excited hydrocarbons and air, but also by the appearance of the first reactions denoted by weak peaks of OH and CH. No heat release is observed at this time.

As the flame front expands (-5.5 CAD), OH radiation grows and becomes very intense, and the chemiluminiscence spectra also show the presence of CH, HCO and HCHO. The resulting spectrum is characteristic of premixed combustion, which is consistent with previously observed RoHR and flame propagation. Soot radiation is only present at the original location where ignition occurred and close to the injector, due to fuel leakages.

After the period of premixed combustion, a transition occurs to an auto-ignition phase induced by compression heating, with a more intense RoHR. Spectra show similar radicals such as HCO and HCOH, while the corresponding OH peak is weaker and CH peaks are more visible than in the previous phase, as a consequence of the change in the combustion regime.

ACKNOWLEDGEMENTS

The authors acknowledge that part of this work was performed in the frame of project DUFUEL TRA2011-26359, funded by the Spanish Government. The authors also thank GM for technical assistance and its support in other parts of this work.

REFERENCES

[1] Yanagihara, H., Sato, Y. and Minuta, J., "A simultaneous reduction in NOx and soot in diesel engines under a new combustion system (Uniform Bulky Combustion System -UNIBUS)", 17th International Vienna Motor Symposium, pp 303-314, 1996.

[2] Kimura, S., Aoki, O., Ogawa, H., Muranaka, S. et al., "New Combustion Concept for Ultra-Clean and High-Efficiency Small DI Diesel Engines," SAE Technical Paper 1999-01-3681, 1999.

[3] Akagawa, H., Miyamoto, T., Harada, A., Sasaki, S. et al., "Approaches to Solve Problems of the Premixed Lean Diesel Combustion," SAE Technical Paper 1999-01-0183, 1999.

[4] Kimura S., Aoki S., Kitahara Y., Aiyoshizawa E. Ultra-clean combustion technology combining a low-temperature and premixed combustion concept for meeting future emission standards. SAE International, SAE 2001-01-0200, 2001.

[5] Mingfa Yao, Zhaolei Zheng, Haifeng Liu, "Progress and recent trends in homogeneous charge compression ignition (HCCI) engines". Progress in Energy and Combustion Science, Volume 35, Issue 5, October 2009, Pages 398-437.

[6] Hanson, R. M., Kokjohn, S. L., Splitter, D. A, and Reitz, R. D. "An experimental Investigation of Fuel Reativity Controlled PCCI Combustion in a Heavy-Duty Engine" SAE international journal of engines, 2010, 3(1) 700-716.

[7] B. Keeler and P. J. Shayler, "Constraints on Fuel Injection and EGR Strategies for Diesel PCCI-Type Combustion". SAE 2008-01-1327.

[8] Yang, J., Culp,T., and Kenney, T. Development of a gasoline engine system using HCCI technology- The concept and the test results. SAE paper 2002-1-2832.

[9] Kalghatgi, G.T., Risberg, P., and Ångström, H.-E., "Advantages of Fuels with High Resistance to Auto-Ignition in Late-Injection, Low-Temperature, Compression Ignition Combustion," SAE Technical Paper 2006-01-3385, 2006.

[10] Kalghatgi, G.T., Risberg, P., and Ångström, H.-E., "Partially Pre-Mixed Auto-Ignition of Gasoline to Attain Low Smoke and Low NOx at High Load in a Compression Ignition Engine and Comparison with a Diesel Fuel," SAE Technical Paper 2007-01-0006, 2007.

[11] Hildingsson, L., Kalghatgi, G., Tait, N., Johansson, B. et al., "Fuel Octane Effects in the Partially Premixed Combustion Regime in Compression Ignition Engines," SAE Technical Paper 2009-01-2648, 2009.

[12] Sjoberg, M and Dec, J.E. "Smoothing HCCI Heat-Release using partial fuel stratification with two-stage ignition fuels". SAE 2006-01-0629, 2006.

[13] H. Persson, A. Rémon, A. Hultqvist, B. Johansson, "Investigation of the early flame development in spark assisted HCCI Combustion Using high speed chemiluminescence Imaging". SAE 2007-01-0212

[14] B. Johansson, "Path to High Efficiency Gasoline Engine". DEER 2010 Lund University.

[15] H. Persson, A. Rémon, B. Johansson, "The effect of swirl on spark assisted compression ignition (SACI)" JSAE20077167, SAE 2007-01-1856 (2007).

[16] Wang, Z., Shuai, S.J., and Wang, J.-X., G-H Tian, Xinliang, Q-J Ma "Study of the effect of spark ignition on gasoline HCCI combustion". Proceedings of the Institution of mechanical Engineers, Part D: Journal of Automobile Engineering. DOI:10.1243/09544070JAUTO151

[17] Vinod K. Natajaran, Volker Sick, David L. Reuus and Gerald Silvas, "effect of spark-ignition on combustion periods during spark assisted compression ignition". Combustion Sci. and Tech, 181:1187-1206,2009

[18] Benajes J, López JJ, Novella R, Garcia A: "Advanced Methodology for Improving Testing Efficiency in a Single-Cylinder Research Diesel Engine"; Experimental Techniques 32:41-47, 2008.

[19] J. Benajes, R. Novella, A. Garcia, V. Domenech, " An investigation on mixing and autoignition using diesel and gasoline in a direct injection compression ignition engine operating in PCCI combustion conditions". SAE Int. J. Engines August 2011 4:2590-2602; doi:10.42712011-37-0008

[20] Lapuerta M, Armas O and Hernández JJ: "Diagnostic of D.I. Diesel Combustion from In-Cylinder Pressure Signal by Estimation of Mean Thermodynamic Properties of the Gas", Applied Thermal Engineering. Vol 19 Nº 5 pp 513–529, 1999.

[21] J.V. Pastor, J.M. Garcia-Oliver, J.M. Pastor, J.G. Ramirez-Hernandez, "Ignition and combustion development for high speed direct injection diesel engines under low temperature cold start conditions". Fuel (2011), doi:10.1016/j.fuel.2011.01.008

[22] Payri F, Molina S, Martín J and Armas O: "Influence of measurement errors and estimated parameters on combustion diagnosis", Applied Thermal Engineering Vol 26 Nº 2-3 pp 226–236, 2006.

[23] Tornatore C., Sementa P., and Merola S.S.: "Optical Investigations of the early combustion phase in spark ignition boosted engines", Proceedings of the Institution of Mechanical Engineers, Part D: Journal of Automobile Engineering, Vol 225; 2011.

[24] Gaydon A.G., The spectroscopy of flame, Chapman and Hall, London, UK, 1957.

[25] Mancaruso E., Vaglieco B. M.: "Spectroscopic measurements of premixed combustion in diesel engine", Fuel Vol. 90, 511-520, 2011.

[26] Kim B., Kaneko M., Ikeda Y., Nakajima T.: "Detailed spectral analysis of the process of HCCI combustion", Proceedings of the Combustion Institute, Vol. 29, 671-677, 2002.

Figure Caption

Fig. 1 – Sketch of the single cylinder optical engine and the modified cylinder head.

Fig. 2 – Optical set-up scheme for registering natural radiation from the combustion reaction.

Fig. 3 – Scheme of processing steps. From left to right: original image, binary image of the flame area and binary image of the flame contour

Fig. 4 – Time evolution of natural luminosity inside the combustion chamber.

Fig. 5 – Crankangle evolution of different variables. From top to bottom: image processed variables (ACV and apparent combustion area), in-cylinder pressure analysis (temperature, pressure and hear release rate), injection rate and spark discharge intensity.

Fig. 6 – Combustion chamber division for chemiluminescence measurements.

Fig. 7 – Spectra registered at 1C between -10.8 and -8.5 CAD

Fig. 8 – Spectra registered at 1C and 2C between -5.5 and -2.3 CAD

Fig. 9– Spectra registered at 1C, 2C and 3C between 2 and 4.3 CAD

Fig.10 – Spectra registered at 2C and 3C between 5.8 and 8 CAD

Figure 1

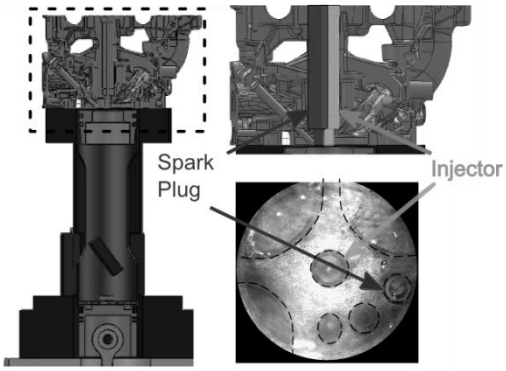

Fig. 2 – Sketch of the single cylinder optical engine and the modified cylinder head.

Figure 2

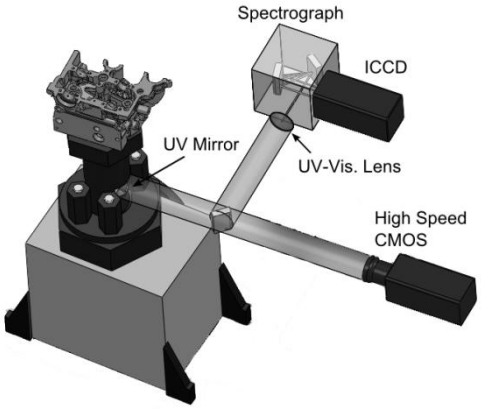

Fig. 3 – Optical set-up scheme for registering natural radiation from the combustion reaction

Figure 3

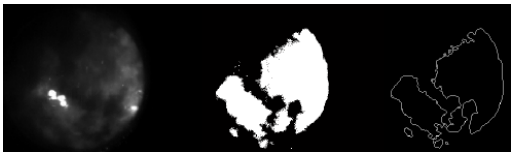

Fig. 4 – Scheme of processing steps. From left to right: original image, binary image of the flame area and binary image of the flame contour

Figure 4

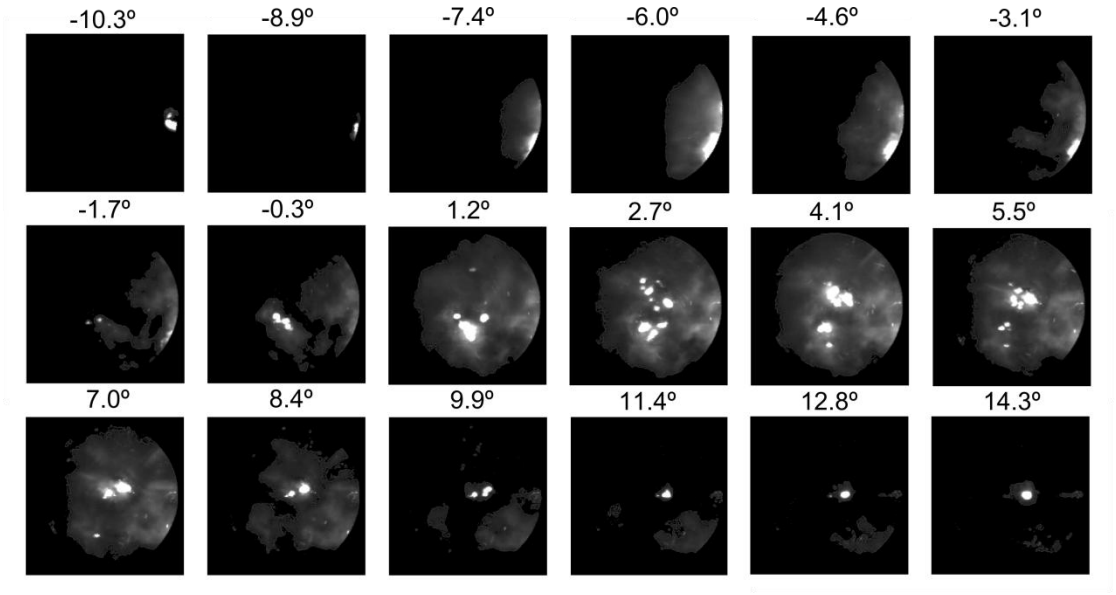

Fig. 5 – Time evolution of natural luminosity inside the combustion chamber.

Figure 5

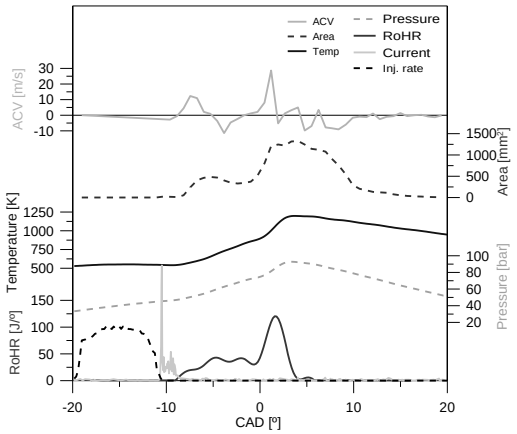

Fig. 6 – Crankangle evolution of different variables. From top to bottom: image processed variables (ACV and apparent combustion area), in-cylinder pressure analysis (temperature, pressure and hear release rate), injection rate and spark discharge intensity.

Figure 6

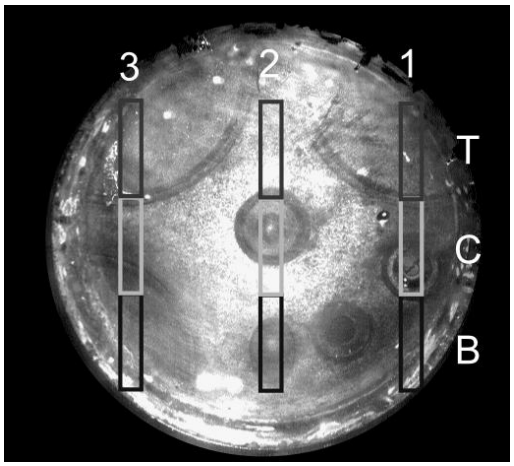

Fig. 7 – Combustion chamber division for chemiluminescence measurements

Figure 7

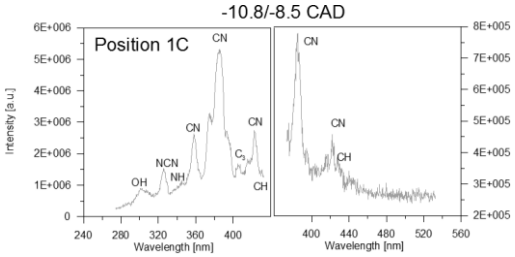

Fig. 7 – Spectra registered at 1C between -10.8 and -8.5 CAD

Figure 8

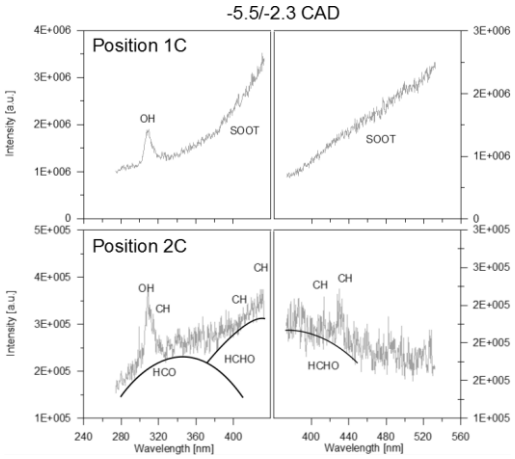

Fig. 8 – Spectra registered at 1C and 2C between -5.5 and -2.3 CAD

Figure 9

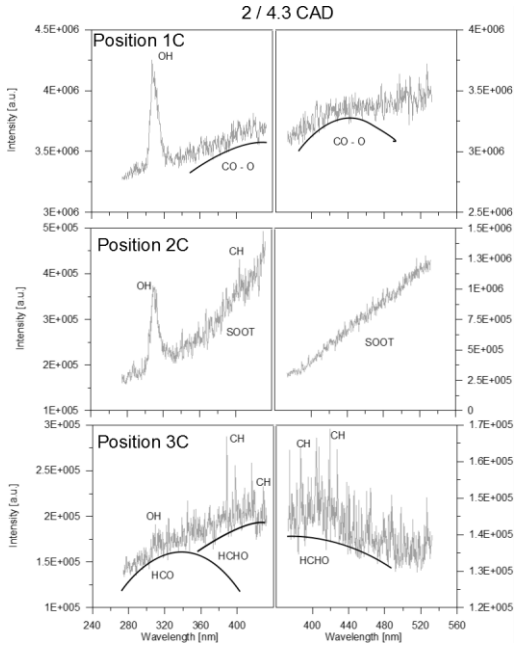

Fig. 9 – Spectra registered at 1C, 2C and 3C between 2 and 4.3 CAD

Figure 10

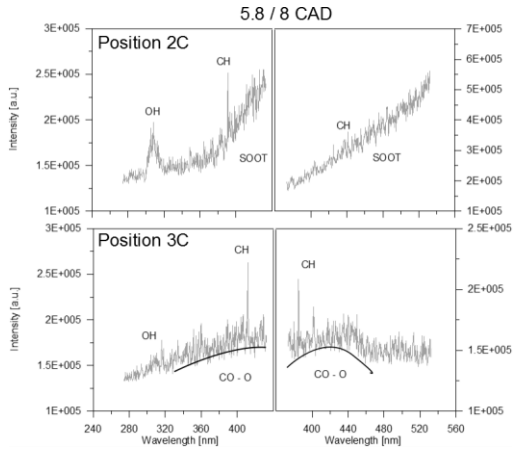

Fig. 10 -Spectra registered at 2C and 3C between 5.8 and 8 CAD

Tables

Table 1

Table1 Engine Specifications

OPTICAL ENGINE	4- Stroke DI Diesel single cylinder
Bore x Stroke (mm)	86 x 96
Displacement (l)	0.5447
Base Compr. Ratio	14.5
Fuel Injection System	Common Rail. Bosch-Piezo System
Nozzle	7 hole – 97 microns – 154º cone angle